Letter of Reply to Referee 1

Thank you for carefully reading the manuscript and providing useful suggestions to improve the paper. We want to summarize the main changes on the manuscript at the beginning and then reply to the specific remarks.

- **Section 4 contains only the statistical overview of the triple-wavelength depolarization observations of long-range transported dust.**
- **A new discussion section (Section 5) is introduced and contains the comparison to previous campaigns (formerly the later part of Section 4) and the discussion of the size information conveyed by the triple-wavelength depolarization measurements (formerly Section 3.1.1)**
- **A meteorological overview of the SALTRACE summer campaigns is added as new Section 2.2.**
- **A short historical overview of the polarization lidar observations of tropospheric dust with the relevant literature was added at the beginning of Section 2.3**
- **The polarization of the 90° mirror in the telescope has been found to have a significant influence on the 532 nm depolarization ratio, so the data and the error estimation has been recalculated. As a result, the 355 and 1064 nm depolarization ratio remained almost unchanged, but the 532 nm values are now decreased by about 0.02 (mean value from 0.30 to 0.28).**
- **The HSRL-2 measurement took place above Missouri and not Arkansas, as our coauthor S. Burton mentioned.**

The changes in the manuscript are marked in bold except of Section 3 (case studies and former Section 3.1.1 now Page 14, Line 28 – Page 15 Line 25 in the discussion), where more things have changed.

Major remarks:

Abstract

SALTRACE-2 does not have to appear in the abstract because it is not used.

SALTRACE-2 is removed from the abstract.

Introduction

The introduction is well constructed and it clearly shows the interest of lidar systems with several polarization channels. The democratization of lidar systems of this type has an interest in the broader atmospheric physics domain, but this can only be done if manpower and money are available, which is far to be the case everywhere. Moreover, there are limitations related to eye safety, to obtain authorizations from air navigation authorities, regardless of location in the world. It would be nice to write a few words about it.

We never included such section in any of our papers during the last decades. So, we decided not to change our way to present our scientific products. So we leave out to discuss eye safety, air navigation, manpower and costs.

About the dust study, please expand the reference list to other groups than the team of the authors. Many others have carried out and published scientific works on the subject of dust.

We agree. The list is expanded (Page 2, Lines 6-15) by several other campaigns studying Saharan dust over Africa and the Atlantic Ocean.

Section 2

The SALTRACE project is very interesting and has been conducted with a relevant approach.

Line 34p6: Why "is not optimized"? Hopefully, there have been many uncertainty studies on BERTHA and it must have a better SNR than POLIS.

BERTHA is a complex lidar system, consisting of 13 receiver channels and several steering mirrors and evolved during the last 20 years step by step. So it is not designed from the beginning to be an excellent polarization lidar. Therefore an appendix for the polarization sensitive characterization of the system is included in this paper. But of course, BERTHA has a more powerful laser and a larger telescope leading to a better SNR. The sentence has been rephrased to make this clear on Page 7 Line 30.

This section refers to Appendix A.

Appendix A

This appendix is quite long, but the results are coming from another article. The calibration process presented is fairly standard in optics. It is laborious and indeed necessary when broad interferential filters (some nm) are used, which integrate temperature sensitive of highly depolarized inelastic scattering lines. But it has been published several times before.

Conversely, it is necessary to give clear information on the stability over time of the calibration. It can evolve with different environmental factors (for example the cleanliness on the optics, the temperature, etc.) and with the aging of certain elements of the detection chain.

Remark: the Mueller matrix computation usually requires precise information on materials and optics in general. That does not seem so easy to obtain. Nevertheless, even if the values are not perfectly accurate, this does not hamper the cited sensitivity study.

The appendix describes the specific properties of the triple-wavelength polarization Raman lidar system and the calculation of the error bars. A detailed description of the lidar system is the basis of the presented results and thus necessary to our opinion. The approach is not new, but published several times before, but it is now applied to the BERTHA lidar system. The broad interference filters are used among other reasons for geometrical reasons of the receiver.

The calibration procedure is described for the final state of the system at the end of the SALTRACE-3 campaign and afterwards back in Leipzig. The temperature of the container was kept constant by a strong air condition. But elements could have degraded over time. In order to see the stability over time, the Rayleigh depolarization in the background (usually between 6 -8 km height) was calculated and showed only slight variations over time. The variation was < 20% for 532 nm and < 30% for 355 nm.

Section 3

This section should be reorganized in order to make it easier for the reader to understand its aim. Between 3 and 3.1, explain that there are 3 case studies and how these different cases are interesting.

Thank you, a short explaining text at beginning of section 3 was added.

Sub-section 3.1 Rename the title to 1st case study: ...

Thank you for this comment. We changed the titles of the subsections to number and name the case studies.

Lines 14-15p8: What parameters are homogeneous? If you are talking about the AOT, this is not the case (see MODIS).

The sentence aimed to state the dust was distributed homogeneously with in the SAL and that the same structure was observed for several days. To not confuse the readers, the passage was deleted.

Lines 18-19p8: This is high for a MBL and actually there can be local effects. The MBL is rather blue in Fig. 2 and the layer above is in the free troposphere. The last one can be created by forcing at the MBL top, linked to the presence of Sc for example. It may be necessary to look at CALIPSO measurements to confirm or disprove this.

This is correct; the MBL does not extend up to 1.75 km. We distinguish between the (convective) marine boundary layer (MBL in blue) and the marine aerosol layer (MAL) which extends up to the trade wind inversion at around 1.75 km. In the absence of Saharan dust above, the MAL consists of marine aerosols only. This is the case in our winter measurements over Barbados (not shown in this paper). In summer the MAL is affected by downward mixing of dust particles. In other publications (for example Jung et al., JGR, 2013) three layers are distinguished: a subcloud layer (up to 500 m), a intermediate layer and the SAL. The passage has been rephrased to avoid misunderstandings (Page 9, Lines 19-21)

Lines 24-25p8 (fig. 3): With 10-day back trajectories, it is more relevant to use the ensemble mode of Hysplit.

We agree and changed Fig 3 and 8 accordingly.

Line 27p8: Provide a reference or explanation for what is called the "classical Raman lidar technique"

It is changed to "conventional Raman technique" and a reference for calculating the extinction and backscatter coefficient independently by using the vibrational Raman lines was added (Page 9, Line 30).

Line 1p9: There are previous references to marine aerosols, for example Flamant et al., JGR, 1998.

Five more references for the marine lidar ratio were added (Flamant et al., 1998; Burton et al., 2012; Dawson et al., 2015; Rittmeister et al., 2017; Haarig et al., 2017) at Page 10, Lines 5-6.

Lines 4-5p9: Why not use what has been found in Fig. 4 to inverse POLIS? BERTHA could also be inverted with Gross et al. (2015) and compared to the previous inversion without using POLIS in order to minimize the polarization calibration effect of both lidars. POLIS seems redundant in this section.

Using the Klett or Raman method to retrieve backscatter and extinction does not affect the volume depolarization ratio, which is the most important to compare the quality of the depolarization measurements. For the particle depolarization ratio, the backscatter coefficient has indeed an influence. The comparison with Polis is shown to demonstrate the accuracy of the depolarization ratios measured with BERTHA, as Polis is an EARLINET reference system with high accuracy (see Freudenthaler's contribution to the 27th ILRC, Freudenthaler, EJP, 2016).

Lines 20-24p9: The error bars overlap and it seems difficult to conclude with certainty.

Sure, but we have POLIS and all the comparison point to the same spectral dependence as we found. Figure 5 is the case study that shows it rather clearly.

In Fig.4, are the error bars including atmospheric variability during the averaging time?

The atmospheric variability is not included in the error bars.

Sub-section 3.2 (instead of 3.1.1) (remove)

This section is more of a discussion and should not be included here. Moreover, it is based only on previous work. It is more a report of the state of the art that has its place in an introduction. The set of values presented comes from Mamouri and Ansmann (2017). It is not clear how this applies to the data used in the article.

We agree that this section fits better to the discussion and moved it to Section 5 (discussion), where the spectral behavior of the depolarization ratio is discussed (Page 14, Line 28 – Page 15 Line 25).

Lines 1-5p10: The aerosol mode ratio changes a lot if you look at AERONET and the values given here can significantly change.

The FMF can vary from day to day (from dust outbreak to dust outbreak). But we do not see these variations within one plume event. We checked always the AERONET observations (before sunset or

briefly after sunrise) closest to our lidar observations, and we did not see any large variability in the FMF.

Lines 20-25p10: This is a conclusion, but not for this article.

It is moved with the section to the discussion and modified slightly.

Sub-section 3.2 (stay section 3.2) The title is not in the topic of the paper. Change the title to 2nd case study: . . .

The title is changed and the case studies are numbered.

Lines 27p10-7p11: This is an important point to check the consistency of the depolarization data between the 3 wavelengths of the BERTHA lidar. This should be placed in a dedicated paragraph, before presenting the case studies. Why did not you evaluate the LRs on your measurements themselves?

Thank you for your suggestion, but we decided to demonstrate the consistency of our three-wavelength depolarization measurements in the presence of a cirrus in this case study. It was the second night measurement of the third SALTRACE campaign, and so it is important to show, that no significant changes in the system occurred within one year. The cirrus was too thin to derive good Raman measurements of the extinction with a meaningful smoothing length. In Section 2.3 a short paragraph was added concerning the cirrus to check the consistency of the depolarization ratios (Page 7, Lines 14-18).

Line 25p11: Could you explain why?

Most probably the dust has a different transport history, now described at Page 11, Lines 10-13. The depolarization ratios for the upper layer (3-4 km) and the lower layer (1.4-3 km) are within the observed variability for dust arriving on Barbados (see Fig. 13),

Sub-section 3.3 Change the title of sub-section 3.3 to: "3rd case study: dust transport from Africa to Arkansas over 12000 km"

The title is changed and the case studies are numbered.

Section 4

In all the text, the meteorological descriptions encountered during the campaigns must be given earlier in the article, for instance after sub-section 2.1.

Thank you for your suggestion. A dedicated subsection 2.2 after the description of the SALTRACE projected was added to describe the meteorological situation.

Lines2-3p14: The sentence is not clear.

The sentence was reshaped (Page 13, Lines 27-31). The 1064-nm depolarization ratio is more sensitive to the large particles, whose fraction might change during long-range transport.

Line 21p14: The differences between these values are in the error bar, thus, the differences are not significant. For the comparison between SALTRACE, SAMUM1 and SAMUM2, are you certain that the dust sources are the same and that the aerosol nature does not change?

The difference in 532nm depolarization ratio is not significant. A note concerning this was added on Page 14, Line 15. We assume that the aerosol source are always the same (west Sahara source) and do not change with time. All our results agree with this assumptions reasonable well.

Lines 1-5p15: there is no change between 532 and 1064 nm from the simulations, why?

The preliminary model calculations based on reasonable shape parametrizations and a rough consideration of the size distribution. The particle coarse mode is probably overestimated in the model. The model is used up to size parameter 10 only, for size parameter > 10 an estimation is necessary. The paragraph Page 15, Lines 30-33, has been reshaped to express the uncertainties in the model assumptions.

Minor remarks:

Line 17p3: lidarstudies to lidar studies
Thank you. It is changed.

Line 18p3: assuarance to assurance

Thank you. It is changed.

Line 30p6:remove V before et al.

Removed.

Line 21p8: 532 nm instead of 1064 nm?

Thank you, indeed the 532 nm volume depolarization ratio is shown.

Line 33p9: 50-60%is it the fine mode fraction?

Yes, it is the fine mode fraction. It is stated more precisely now.

Line 12p10: What observations?

Now, that this paragraph is placed in the discussion, it gets clearer. The observations are the spectral depolarization ratio measurements of long-range transported dust.

Line 17p10: diameter inthe. . .

Thank you, it is corrected.

Line 17p11: replace equal by very close

Replaced.

Lines 32p10-2p12: Not useful for the paper.

We deleted the paragraph and recommend studying Mamouri and Ansmann, 2017

Lines 5 and 9p12: Cite the figures in order of appearance

Thank you, we changed the order of figures.

Line 7p13: remove"see sect. 2.4", not useful

Removed.

Lines 18-19p13: already said

But to our opinion it is good to say it at this part again.

Line 20p17: amtmospheric to atmospheric

Changed, thank you.

Table 3: define each variable in the table caption.

The variables are now defined in the caption of the table to make it easier for the reader.

Letter of Reply to Referee 2

Thank you for carefully reading the manuscript and providing useful suggestions to improve the paper. We want to summarize the main changes on the manuscript at the beginning and then reply to the specific remarks.

- **Section 4 contains only the statistical overview of the triple-wavelength depolarization observations of long-range transported dust.**
- **A new discussion section (Section 5) is introduced and contains the comparison to previous campaigns (formerly the later part of Section 4) and the discussion of the size information conveyed by the triple-wavelength depolarization measurements (formerly Section 3.1.1)**
- **A meteorological overview of the SALTRACE summer campaigns is added as new Section 2.2.**
- **A short historical overview of the polarization lidar observations of tropospheric dust with the relevant literature was added at the beginning of Section 2.3**
- **The polarization of the 90° mirror in the telescope has been found to have a significant influence on the 532 nm depolarization ratio, so the data and the error estimation has been recalculated. As a result, the 355 and 1064 nm depolarization ratio remained almost unchanged, but the 532 nm values are now decreased by about 0.02 (mean value from 0.30 to 0.28).**
- **The HSRL-2 measurement took place above Missouri and not Arkansas, as our coauthor S. Burton mentioned.**

The changes in the manuscript are marked in bold except of Section 3 (case studies and former Section 3.1.1 now Page 14, Line 28 – Page 15 Line 25 in the discussion), where more things have changed.

General Comments:

This paper deals with triple-wavelength depolarization ratio measurements performed in aged Saharan dust layers, highlighting the importance of multi wavelength polarization observations for dust modeling improvements and dust characterization. The authors rightly acknowledge previously reported studies, related to field/laboratory observations and to modeling simulations.

The manuscript is well written, discussing interesting measurements, and worth being published in Atmospheric Chemistry and Physics, under the SALTRACE project. However, in order to be improved, I would suggest to the authors to take into consideration the following comments.

Major remarks:

1. The introduction is well written providing a good overview. In my opinion in this section should be also mentioned that airborne triple-wavelength depolarization measurements of Saharan dust in Caribbean exist in the literature by Burton et al., 2015. However, this is something that is mentioned later in section 2 (Page 4, Line 33). Moreover, in this section, should be made clearer to the reader which is the focus of this manuscript.

You are right; the focus of the paper is strengthened by adding a paragraph in the introduction (Page 3, Lines 21-24). It is good to mention the Burton study already in the introduction. We add it on Page 3, Lines 19-21.

2. Page 6, Line 34: Could you please comment briefly in which sense BERTHA was not optimized for depolarization observations?

BERTHA is a complex lidar system, consisting of 13 receiver channels and several steering mirrors and evolved during the last 20 years step by step. So it is not designed from the beginning to be an excellent polarization lidar. Therefore an appendix for the polarization sensitive characterization of the system is included in this paper. The sentence has been rephrased to make this clear on Page 7 Line 30.

3. Page 7, Line 15: To my understanding, for characterizing CALIOP observations as dust or not, a threshold value has been set regarding the particle depolarization ratio. Two lines later is mentioned that "only the observations characterized as dust or polluted dust from the CALIPSO…". In case that are used also scenes characterized as polluted dust, then lower values of particle depolarization ratios are introduced to the statistics. Could you please comment more on this and make it clearer?

We thank the reviewer for this comment. We re-calculated CALIPSO means using only the observations characterized as dust. The new CALIPSO means are higher by 0.01 above Barbados and Cape Verde, while above Morocco are identical. We change the corresponding text in the manuscript: Page 8, Line 11: "only the observations characterized as dust from the CALIPSO"

4. The focus of the manuscript is to demonstrate triple-wavelength depolarization measurements of dust particles, through three case studies. These case studies have to be well organized and demonstrated in the manuscript, in order to be easier for the reader to follow up. Thus, I suggest to the authors to rename the sub-section headers accordingly. For example the 3.1 could be something like: "Case study I: 11 July 2013".

Thank you for this comment. We changed the headers of the subsections to number and name the case studies.

5. Page 8, Line 29: The authors are mentioning that the backscatter coefficient at 1064 nm is significantly lower than the corresponding values at 532 nm. This seems to be more intense during the first case study, compared to the next two. How could this be further explained? The temporal evolution of columnar Angstrom exponent (500/1020 nm) as obtained from the corresponding AERONET site, indicate a variability around 0.1-0.2. This seems to be in contradiction with the high backscatter related Angstrom exponent derived from 532 and 1064 nm (Fig. 4; around 0.5 in the SAL). Higher backscatter coefficient at 1064 nm, would lead to different spectral dependence of particle linear depolarization ratio at the wavelength pair of 1064 to 532 nm (Fig. 5c). By the way, I think that it would be beneficial for the manuscript if for each case study, the corresponding columnar AERONET observations, are also presented.

Thank you for your helpful comment. We carefully checked all our data, especially the reference values for the 1064 nm backscatter. As a result we updated Fig. 4. Additionally, the corresponding AERONET observations are now given for all case studies in Fig. 4, 9 and 12.

6. The sub-section 3.1.1 is really interesting and provides valuable information for the findings presented in this study. However, in my opinion should be moved either in a separated paragraph in section 2 as a generic methodology followed during SALTRACE project to provide complementary dust related information, or has to be shorten in order to be directly included in the sub-section 3.1 which describes the Case I. Moreover, I think that the last paragraph (Page 10, Lines 20-25) of this sub-section is more related to the Conclusions section, than here.

We moved this subsection to the discussion (section 5, Page 14, Line 28 – Page 15 Line 25), because it discusses our three-wavelength depolarization observations and sets them in a broader context.

7. As already mentioned (see major remark No. 4) you are kindly suggested to change the header of sub-section 3.2 to something like: "Case study II: 20-21 June 2014". Moreover, in my opinion a dedicated paragraph should be constructed earlier than section 3, in order to demonstrate the consistency of the depolarization data between the 3 wavelengths of the BERTHA lidar. This paragraph could include the comparison with POLIS and the cirrus case presented in Figures 5 and 6.

The subsection header was changed. We decided to not construct a separate paragraph to show the consistency of our depolarization data, but to use the case studies to demonstrate this. To check the results with a reference system or to use a cirrus case, is a normal tool that should be used always and thus is part of a case study. In this way the case studies give an idea about the vertical structure of dust layer over Barbados and indicate the quality of our depolarization measurements. In Section 2.3 a short paragraph was added concerning the cirrus to check the consistency of the depolarization ratios (Page 7, Lines 14-18).

8. Why in Fig. 6b the volume depolarization profiles at 532 and 1064 nm are not plotted above the cirrus? Is this due to signal to noise issues of the corresponding cross-polarized channels? Moreover, if the volume depolarization ratio is equal to particle depolarization ratio at 1064 nm, this is something that should be mentioned in the caption of Fig. 6b.

The volume depolarization ratio becomes noisy above the cirrus and was therefore not plotted. A sentence to the volume and particle depolarization ratio at 1064 nm was added to the caption of Fig 6b.

9. In Fig. 14 it would be nice also to show the number of case studies used for the corresponding statistical values obtained with BERTHA, MULIS and POLIS during SALTRACE and SAMUM 1-2.

We went through the reference and added the information. For SAMUM 1 and 2, there were not so many cases. The information is added in the caption of Fig. 14.

10. In my opinion Fig. 15 is an important figure summarizing all the scientific results and open questions of the manuscript. The scientific answers which are related to the less sharp (compared to observations)

simulated dust depolarization spectral slopes, along with the discrepancies found in HSRL-2 and BERTHA observations (which are inverted when going to higher wavelengths) are scattered in the manuscript, but not well summarized when describing Fig. 15.

Thank you for pointing this out. By moving Section 3.1.1 to the discussion and discuss the spectral slope in this separate Section, the focus is strengthened in Section 5.

Minor Remarks:

1. Page 3, Line 17: Change "lidastudies" to "lidar studies".

Thank you. It is changed.

2. Page 5, Lines 8-9: It is clear from Fig. 1 that the linear polarizers are behind the beam expanders however, you could mention this also in the manuscript. Moreover, it would be helpful if you could describe if there is a specific need for using two lasers in BERTHA setup? Is this due to the implemented HSRL channel at 532 nm, or is related to the plane of polarization of each laser generated harmonic?

The comment on the position of the linear polarizer was added (Page 5, Line 29). In fact a linear polarizer after the beam expander would be a good idea, but it is technically challenging because of a beam diameter of around 10 cm. Two lasers are used for two reasons, firstly to have a frequency stabilized 532-nm laser for the implementation of the HSRL-channel and secondly to have a backup laser in the field campaign (Page 5, Lines 32-33).

3. Page 6, Line 30: "Freudenthaler, V. et al., 2016" delete the "V.".

Deleted.

4. Page 7, Line 31: I kindly suggest changing the AERONET site name with the one that can be found in AERONET website, namely Barbados_Saltrace.

The site name is indicated (Page 8, Line 26)

5. Page 8, Line 21: In the manuscript, the wavelength of 1064 nm is mentioned while in Fig. 2 and its caption the 532 nm is shown. Please consider correcting where appropriately.

The text has been changed to "532 nm".

6. Page 8, Line 27: I would suggest replacing the text "classical Raman" with "conventional Raman".

It is changed to "conventional Raman" and a reference is provided (Page 9, Line 30).

7. Page 8, Line 28: Since there are many studies of Saharan dust observations with conventional Raman systems, I would suggest to the authors to provide some more references than "Tesche et al., 2011a".

We agree; there are many observations. The reference list has been extended by Mattis et al., 2002; Papayannis et al., 2005; Tesche et al., 2011a; Preißler et al., 2011; Veselovskii et al., 2016; Hofer et al., 2017 (Page 9, Line 31 – Page 10, Line 1). But there are many more Raman lidar observations of dust.

8. Page 9, Line 18: Please consider providing same number of significant digits for common parameters. This is a general comment and I would suggest go over the entire manuscript and tables, in order to correct it where appropriately.

Thank you, we went through the manuscript and unified the number of significant digits. For the particle linear depolarization ratio we use normally 2 significant digits (for an overall average 3), for the volume depolarization ratio in the Rayleigh background we need 4 digits.

9. Page 9, Line 29: Delete the word "here" due to redundancy.

Deleted.

10. Page 11, Line 3: "BERTHA was operated at…this measurement". This information has been already provided earlier (page 5, line 10). I suggest you to delete it from here.

The passage has been deleted.

11. Page 13, Line 31: Change "give" to "given".

Changed.

12. Page 17, Line 12: A definite article "the" is missing.

It was added, thank you.

Triple-wavelength depolarization-ratio profiling of Saharan dust over Barbados during SALTRACE in 2013 and 2014

Moritz Haarig[1], Albert Ansmann[1], Dietrich Althausen[1], André Klepel[1,2], Silke Groß[3],
Volker Freudenthaler[4], Carlos Toledano[5], Rodanthi-Elisavet Mamouri[6], David A. Farrell[7], Damien
A. Prescod[7], Eleni Marinou[8], Sharon P. Burton[9], Josef Gasteiger[10], Ronny Engelmann[1], and
Holger Baars[1]

[1]Leibniz Institute for Tropospheric Research, Leipzig, Germany
[2]Goldschmidt Thermit GmbH, Technology Innovation Center, Leipzig, Germany
[3]German Aerospace Center, Institute of Atmospheric Physics, Oberpfaffenhofen, Germany
[4]Ludwig Maximilians University, Meteorological Institute, Munich, Germany
[5]University of Valladolid, Group of Atmospheric Optics, Valladolid, Spain
[6]Cyprus University of Technology, Department of Civil Engineering and Geomatics, Limassol, Cyprus
[7]Caribbean Institute for Meteorology and Hydrology, Bridgetown, Barbados
[8]Inst. for Astronomy, Astrophysics, Space Appl. and Remote Sensing, National Observatory Athens, Athens, Greece
[9]NASA Langley Research Center, MS 475, Hampton, VA 23681, USA
[10]University of Vienna, Aerosol Physics and Environmental Physics, Vienna, Austria

Correspondence to: Moritz Haarig (haarig@tropos.de)

Abstract. Triple-wavelength polarization lidar measurements in Saharan dust layers were performed at Barbados (13.1°N, 59.6°W), 5000–8000 km west of the Saharan dust sources, in the framework of the Saharan Aerosol Long-range Transport and Aerosol-Cloud-Interaction Experiment (SALTRACE-1, June-July 2013, SALTRACE-3, June-July 2014). Three case studies are discussed. High quality was achieved by comparing the dust linear depolarization ratio profiles measured at 355, 532, and 1064 nm with respective dual-wavelength (355, 532 nm) depolarization ratio profiles measured with a reference lidar. A unique case of long-range transport dust over more than 12000 km is presented. Saharan dust plumes crossing Barbados were measured with an airborne triple-wavelength polarization lidar over **Missouri** in the Midwestern United States 7 days later. Similar dust optical properties and depolarization features were observed over both sites indicating almost unchanged dust properties within this one week of travel from the Caribbean to the United States. The main results of the triple-wavelength polarization lidar observations in the Caribbean in the summer seasons of 2013 and 2014 are summarized. On averaged, the particle linear depolarization ratios for aged Saharan dust were found to be **0.252±0.030 at 355 nm, 0.280±0.020 at 532 nm, and 0.225±0.022 at 1064 nm** after approximately one week of transport over the tropical Atlantic. Based on published simulation studies we present an attempt to explain the spectral features of the depolarization ratio of irregularly shaped mineral dust particles, and conclude that most of the irregularly shaped coarse-mode dust particles (particles with diameters >1 μm) have sizes around 1.5–2 μm. The SALTRACE results are also set into the context to the SAMUM-1 (Morocco, 2006) and SAMUM-2 (Cabo Verde, 2008) depolarization ratio studies. Again, only minor changes in the dust depolarization characteristics were observed on the way from the Saharan dust sources towards the Caribbean.

1 Introduction

Mineral dust belongs to the major natural atmospheric aerosol components and influences weather and climate, visibility, air quality, and human health. Large efforts are undertaken to develop sophisticated dust transport models to provide predictions of dust occurrence, vertical distribution of dust particles and their impact on the Earth's radiation field, cloud formation, and environmental/air-quality conditions (Huneeus et al., 2011; Heinold et al., 2011; Garimella et al., 2014; Solomos et al., 2017). **A variety of features of the impact of dust on (climate-relevant) atmospheric processes are not well understood and represented in atmospheric models, and thus need to be explored, preferably in comprehensive field campaigns such as Aerosol Characterization Experiment ACE-Asia (Huebert et al., 2003; Shimizu et al., 2004), the Puerto Rico Dust Experiment PRIDE (Colarco et al., 2003; Reid et al., 2003), the Saharan Dust Experiment SHADE (Tanré et al., 2003), the Saharan Mineral Dust Experiments SAMUM-1 (Heintzenberg, 2009) and SAMUM-2 (Ansmann et al., 2011), the Dust and Biomass-burning Experiment DABEX (Haywood et al., 2008), the Dust Outflow and Deposition to the Ocean project DODO (McConnell et al., 2008), the Geostationary Earth Radiation Budget Intercomparisons of Long-wave and Short-wave radiation GERBILS (Johnson and Osborne, 2011), Fennec (Ryder et al., 2013), the Saharan Aerosol Long-Range Transport and Aerosol-Cloud-Interaction Experiment SALTRACE (Weinzierl et al., 2017) and the Study of Saharan Dust Over West Africa SHADOW (Veselovskii et al., 2016).**

Besides a precise description of dust in atmospheric models, there is also a strong need for a better knowledge of the link between the microphysical and optical dust properties to improve dust profiling and retrieval techniques (Veselovskii et al., 2010, 2016; Müller et al., 2013; Lopatin et al., 2013; Chaikovsky et al., 2016; Bovchaliuk et al., 2016). Recently, a new aerosol retrieval technique was proposed, which makes use of depolarization-ratio profiling and permits the separation of fine dust, coarse dust, and residual (marine or anthropogenic) aerosol profiles in terms of light backscatter, extinction, and mass concentration (Mamouri and Ansmann, 2014). Based on SALTRACE triple-wavelength polarization measurements, it is investigated at which of the three wavelengths this new method works best and the uncertainties are lowest Mamouri and Ansmann (2017).

One of the fundamental open questions **regarding the influence of mineral dust on climate** is related to the specific impact of the size, shape, **and chemical** composition characteristics of desert dust particles on light scattering and depolarization (Dubovik et al., 2006; Wiegner et al., 2009; Müller et al., 2010b, a, 2012; Gasteiger et al., 2011; Kemppinen et al., 2015a, b). Besides modeling studies and field observations, laboratory experiments contribute to this field of research (West et al., 1997; Volten et al., 2001; Liu et al., 2003; Curtis et al., 2008), recently also with focus on lidar applications (Sakai et al., 2010; David et al., 2013; Miffre et al., 2016; Järvinen et al., 2016). Although significant progress is made during the last decade, models describing the scattering properties of desert dust particles from forward scattering to backward scattering (up to angles of exactly 180°) need a number of assumptions especially about the particle morphology and composition when explaining the optical effects gained from active and passive remote sensing at different wavelength from the UV to IR (Gasteiger et al., 2011; Kemppinen et al., 2015a, b). Observations of dust optical properties are in strong contradiction with model simulations when a spherical dust particle shape model is applied. The widely used and accepted approach to describe dust particles as spheroids works well in the case of sun photometer retrievals (Dubovik et al., 2006). However, significant uncertainties in

the observational products arise whenever lidar measurements (and thus 180° scattering processes) come into play and are included in the data analysis in which a spheroidal shape model is used (Wagner et al., 2013; Veselovskii et al., 2010, 2016; Müller et al., 2013). There is a clear need for complex efforts of simulation studies, laboratory investigations, and field observations in order to better parametrize the relationship between the dust particle shape and size distribution characteristics and the scattering phase function with emphasis on depolarization and scattering at high scattering angles. **The depolarization ratio observed with lidar is rather sensitive to the dust particle shape (Gasteiger et al., 2011; Kemppinen et al., 2015a). The spectral dependence of depolarization, as presented in this article, contains in addition information on the dust size spectrum. Thus triple-wavelength depolarization ratio observations are of great value for the optical modeling community (Gasteiger and Freudenthaler, 2014) and support efforts to develop realistic dust shape models, which are not available yet. In the first stage, however we have to demonstrate that triple-wavelength depolarization observations can be successfully performed.**

To contribute to this field of dust research, we re-designed and upgraded our multiwavelength polarization/Raman lidar BERTHA (Backscatter Extinction lidar-Ratio Temperature Humidity profiling Apparatus) (Althausen et al., 2000; Tesche et al., 2009; Haarig et al., 2016b). BERTHA has been used in nine field campaigns in Europe, Asia, and Africa from 1997–2008 (Wandinger et al., 2002; Ansmann et al., 2002; Franke et al., 2003; Tesche et al., 2009, 2011a). We implemented new channels to permit simultaneous observations of dust linear depolarization ratios at 355, 532, and 1064 nm. Freudenthaler et al. (2009) and Burton et al. (2015) showed already that the dust linear depolarization ratio significantly changes with the transmitted laser wavelength, obviously as a result of changing contributions of fine-mode dust particle (particles with diameters <1 μm) and coarse-mode (super-micrometer) particles to the light depolarization. **Burton et al. (2015) recently presented triple-wavelength polarization lidar observations in an aged and fresh dust layer performed with an airborne high spectral resolution lidar (HSRL-2). The main goal of the paper is to present for the first time ground-based triple-wavelength polarization/Raman lidar observations (case studies) of the depolarization ratio of Saharan dust after long range transport and to provide a high-quality statistical data set of dust depolarization ratios at 355, 532, and 1064 nm.** We conducted three campaigns on the Caribbean island of Barbados in the framework of SALTRACE. Two of them took place in the summer seasons of 2013 (**SALTRACE-1**) and 2014 (**SALTRACE-3**) to study Saharan dust layers advected from Africa towards North America. The third field campaign (**SALTRACE-2**) was performed in February-March 2014 to continue our research on mixed dust and smoke transport towards America during the winter half year (Ansmann et al., 2009; Baars et al., 2011; Tesche et al., 2011b; Rittmeister et al., 2017).

We begin our SALTRACE report with a short description of the SALTRACE experiment and instrumentation. The main part of Sect. 2 (and the Appendix) deals with the explanations of the triple-wavelength polarization lidar BERTHA. The results are presented in Sects. 3 and 4. In Sect. 3, three case studies are discussed. A statistical overview of the SALTRACE depolarization measurements is given in Sect 4. The findings are compared with respective results from the foregoing SAMUM-1 and SAMUM-2 field campaigns **and the Cloud-Aerosol Lidar with Orthogonal Polarization (CALIOP) satellite observations in the discussion Section 5**. Concluding remarks are given in Sect. 6.

3

2 SALTRACE campaigns and instrumentation

2.1 The SALTRACE project

The SALTRACE field campaigns performed in the summer of 2013 and in the winter and summer of 2014 belong to the SAMUM-SALTRACE field campaign series. As shown and illustrated in Fig. 7 of Weinzierl et al. (2017), six comprehensive dust field campaigns have been conducted since 2006: SAMUM-1, SAMUM-2a and 2b, and SALTRACE-1, 2, and 3. The Saharan Mineral Dust Experiment (SAMUM) project SAMUM-1 (Heintzenberg, 2009) took place in southern Morocco (May-June 2006) to investigate the role of freshly emitted dust in the climate system. SAMUM-2 (Cabo Verde, SAMUM-2a, January-February 2008, SAMUM-2b, May-June 2008) (Ansmann et al., 2011) investigated the dust physico-chemical, optical, and radiative properties of mixtures of biomass burning smoke and mineral dust (SAMUM-2a, winter transport regime) and of pure dust (SAMUM-2b, summer transport mode) after an atmospheric transport over 1000-3000 km (1-3 days after emission). During SALTRACE, we investigated the dust properties after an atmospheric travel over 5–12 days and 5000–8000 km (Weinzierl et al., 2017).

As the logistically favorable field site for lidar observations we selected the Caribbean Institute of Meteorology and Hydrology (CIMH, 13.1°N, 59.6°W, 90 m above sea level) in Husbands, in the northern parts of the capital Bridgetown at the west coast of Barbados. The station is not influenced by any local (island) anthropogenic pollution because of the steady northeasterly airflow and the absence of pollution sources in the northern part of Barbados upwind the lidar station. In the summer months of June and July (SALTRACE-1 and 3), transported dust layers were observed. The SALTRACE lidar activities were complemented by shipborne observations along the main Saharan dust transport route over the tropical North Atlantic in April-May 2013 (Kanitz et al., 2014; Rittmeister et al., 2017; Ansmann et al., 2017), in situ observations of microphysical (size distribution, mass concentration, particle shape), chemical, and optical aerosol properties at Ragged Point (20 km east of CIMH) at the east coast of Barbados (Kristensen et al., 2016; Wex et al., 2016) and airborne in situ aerosol observations and Doppler lidar measurements of aerosol layering and atmospheric wind fields (Chouza et al., 2015, 2016a, b; Weinzierl et al., 2017). The SALTRACE in situ observations include studies of the efficiacy of aged desert dust to serve a cloud condensation nuclei (Kristensen et al., 2016; Wex et al., 2016; Weinzierl et al., 2017), and modeling studies of dust transport across the Atlantic (Chouza et al., 2016a; Ansmann et al., 2017) and the impact of the Caribbean island on the airflow and downward mixing of dust (Jähn et al., 2016; Chouza et al., 2016b).

2.2 Meteorological Conditions

In Rittmeister et al. (2017), the dust transport from Africa towards the Caribbean is discussed. The main features of dust layering across Atlantic described by the conceptual model (Karyampudi et al., 1999) are illuminated and compared with the shipborne SALTRACE lidar observations. According to the conceptual model (Karyampudi et al., 1999) hot, dry, dust-laden air masses emerge from the western coast of Africa as a series of large-scale pulses in the summer months. Associated with easterly wave activity, Saharan dust outbreaks occur as discrete episodic pulses, which generally last 3–5 days. These dust outbreaks are mostly confined to a well-mixed layer, the Saharan air layer (SAL), that

often extends to 5–6 km in height over West Africa due to intense solar heating in summer months. The airborne dust is carried westward by the prevailing easterly flow in the latitude belt of $10°$–$25°$N. As the dust plumes are advected further west in the predominantly easterly flow, the base of the SAL rises rapidly as it is undercut by the relatively clean northeasterly trade winds. The well-mixed SAL resides above the trade wind inversion layer which is on top of the marine aerosol layer (MAL). The dust transport takes usually 5–7 days across the Atlantic. The strong temperature inversion at the base of the SAL limits convective activity and consequently precludes the possibility of strong wet deposition, except during periods with deep convection and precipitation.

2.3 Triple-wavelength polarization lidar BERTHA

We begin with a short historical overview of polarization lidar observations of tropospheric dust. The polarization lidar technique was applied to tropospheric aerosols for the first time in the early 1970s (McNeil and Carsweil, 1975). Systematic measurements of the depolarization ratio in desert dust layers started in the 1980s in eastern Asia (Kobayashi et al., 1985; Iwasaka et al., 1988) and demonstrated the importance of polarization lidar for dust monitoring. Consequently, the Asian Dust Lidar Network was established in the 1990s (Murayama et al., 2001; Shimizu et al., 2004). In Europe, systematic Saharan dust studies with polarization lidars began in the 1990s (Gobbi, 1998; Gobbi et al., 2000; di Sarra et al., 2001). Dust was investigated later on by means of polarization lidar in the framework of the European Aerosol Research Lidar Network (e.g., Ansmann et al., 2003)). All of the ground-based observations, conducted before SALTRACE, were based on single-wavelength lidar observations, although several single-wavelength-lidar systems were combined during dedicated field campaigns such as SAMUM-1 and 2 (Freudenthaler et al., 2009; Groß et al., 2011b; Tesche et al., 2011a). In the majority of applications the laser wavelength was 532 nm. Sugimoto and Lee (2006) presented the first ground-based dual-wavelength polarization lidar observations of dust performed at 532 and 1064 nm. Airborne dual-wavelength polarization lidar observations (at 532 and 1064 nm) were realized in Saharan dust aboard the Falcon of the Germany Aerospace Center during SAMUM-1 in 2006 (Freudenthaler et al., 2009). During SALTRACE, dual-wavelength polarization lidars were operated simultaneously at 355 and 532 nm (Kanitz et al., 2014; Groß et al., 2015; Rittmeister et al., 2017). And recently the first triple-wavelength polarization lidars were developed and performed dust observations at 355, 532, and 1064 nm aboard an aircraft (Burton et al., 2015) and at ground (Haarig et al., 2016a).

The schematic structure of the lidar system BERTHA is shown in Fig. 1. Two Nd:YAG lasers transmit linearly polarized laser pulses at 355 and 1064 nm (first laser) and at 532 nm (second laser) with a repetition rate of 30 Hz. Two linear polarizers are installed **behind the laser and before the beam expander** to further clean the polarization of the outgoing light. The pulse energies can be as high as 1000 mJ (1064 nm), 800 mJ (532 nm) and 120 mJ (355 nm) in the ideal case of well-working optical elements in the transmission unit of the lidar. However, the pulse energies were only about 50% of these maximum values during the SALTRACE campaigns. **Two lasers are used for two reasons, firstly to have a frequency stabilized 532 nm laser for the implementation of the HSRL-channel and secondly to have a backup laser in the field campaign.** The laser beams are aligned on an optical axis and directed through a beam expander. The beams are expanded tenfold and

afterwards pointed into the atmosphere at an off-zenith angle of $5°$. By using a tilt angle of $> 3°$ specular reflection by falling and horizontally aligned ice crystals does no longer influence the measurements as our experience shows.

A Cassegrain telescope with 53 cm diameter collects the backscattered light. The receiver field of view is 0.8 mrad. To avoid overloading of the photomultipliers (PMTs, photon counting mode) in the near range we restricted the maximum count rate to 20 MHz for the signal maximum in about 500 m height **by means of neutral density filters**.

The receiver unit was completely re-designed to measure the **linear** depolarization ratio at all three wavelengths. In addition, a high spectral resolution (HSR) channel was added (see Fig. 1). All detectors are photomultiplier tubes (PMT) working in the photon counting mode (H10721P-110 from Hamamatsu). But for the 1064 nm channels the PMT R3236 from Hamamatsu are used at a temperature below $-30°C$ to reduce signal noise in the near infrared. The elastic backscatter signals (total signals) as well as the so-called cross-polarized signal components are detected at the three emitted wavelengths (355, 532, 1064 nm). Polarization filters, each adjusted orthogonal to the plane of linear polarization of the outgoing laser pulses, are placed in front of the detectors which enable the detection of the cross-polarized laser radiation at the three wavelengths. For these six elastic channels, interference filters with 1 nm FWHM (full width at half maximum) are placed in front of each PMT. The vibrational-rotational Raman signals at 387 and 607 nm (nitrogen) and 407 nm (water vapor, night time only) are detected as well. Interference filters with 3 nm FWHM are used at the Raman wavelengths. A double-grating monochromator enables the detection of pure rotational Raman signals from nitrogen and oxygen (J0, J6 and J12) from the 532 nm emission wavelength. Neutral density filters are placed in front of each detector to adjust the signal to the linear range of the detector to avoid dead time effects of the photo multipliers. Nevertheless the PMTs are tested in the lab to correct high counting rates for dead time effects if necessary (Engelmann et al., 2016).

The signals are detected with a range resolution of 7.5 m and a time resolution of 5 to 30 s. A camera is used to **visualize** the overlap between the 532 nm laser beam and the receiver field of view. **The camera is permanently placed in the position of a receiving channel (see Engelmann et al., 2016).** Complete overlap is reached at 800–1000 m for the 532 nm related channels and approximately at 1500 m for the 355 nm-related channels. The 355 and 532 nm backscatter coefficient is derived from the ratio of the elastic backscatter signal to the respective nitrogen Raman signal (387 or 607 nm) and therefore not much affected by the overlap profile. Even at 1064 nm we used the nitrogen Raman signal at 387 nm as the reference signal in the 1064 nm backscatter retrieval. Both signals are caused by backscattered laser-1 photons (see Fig. 1) so that almost the same overlap characteristics holds for both signals and the overlap effects widely cancels out when forming the signal ratio. We used the sun photometer observations (Sect. 2.6) of the spectral slope of aerosol extinction for the correction of minor differential (387 nm vs 1064 nm) particle extinction effects in the backscatter retrieval. On clear (dust-free) days we checked the overlap function according to Wandinger and Ansmann (2002). Trustworthy results can be obtained at altitudes above about 400 m for the backscatter coefficient and above about 1000 m for the extinction coefficient, derived from the 387 and 607 nm nitrogen Raman signal profiles.To control the correct alignment, a telecover test (Freudenthaler, 2008) with 8 segments (4 inner and 4 outer) has been performed during SALTRACE-2 and at Leipzig in the autumn of 2014.

The focus of this article is on depolarization-ratio observations. In order to ensure a high quality of the data, the polarization sensitivity of the lidar system was characterized carefully. The polarization sensitive transmission of the optical elements in

the emitter and the receiver has been characterized. A detailed description of the polarization characterization can be found in Appendix A.

The basic lidar-derived quantity is the volume linear depolarization ratio defined as the ratio of **cross- to co-polarized signal components (Gimmestad, 2008)**. Co and cross denote the planes of polarization (for which the receiver channels are sensitive) parallel and orthogonal to the plane of linear polarization of the transmitted laser pulses, respectively. In the case of BERTHA we measure the cross-polarized and total (cross + co-polarized) signal components and thus determined the co-polarized signal component from the cross-polarized and total signal components (more details are given in the Appendix).

The volume depolarization ratio at 355 and 532 nm is influenced by light depolarization by air molecules, aerosol, and cloud particles. To obtain the particle depolarization ratio a correction for **molecular** depolarization effects have to be applied (Biele et al., 2000). To account for **molecular** backscatter, extinction and depolarization contributions to the measured lidar signals we used the SALTRACE radiosonde observations at CIMH, which were performed twice a day (Sect. 2.7). The radiosonde height profiles of air temperature and pressure profiles permit the computation of the actual height profile of air molecule number concentration over Barbados.

The presence of cirrus is routinely used to check the consistency of the depolarization ratios at different wavelengths among each other. Because the size of the ice crystals is usually much larger than the laser wavelength, the measured optical properties are close together for the 355 to 1064 nm wavelength range. This can be used to evaluate the quality of the depolarization ratio observations for each of the three wavelengths. Case study II in the next section will be an example for these routine checks.

An extended analysis of **systematic** uncertainties in the retrieved optical properties can be found in Freudenthaler et al. (2009); Freudenthaler (2016); Tesche et al. (2009, 2011a, b); Bravo-Aranda et al. (2016). The error bars of the retrieval products given in the next sections show standard deviations considering the overall uncertainty.

2.4 POLIS

During the SALTRACE-1 campaign in the summer of 2013, the dual-wavelength polarization lidar POLIS (Portable Lidar System) of the Munich University (Groß et al., 2015) was operated at CIMH, about 50 m north of the BERTHA lidar. POLIS is a well-designed and characterized six-channel polarization/Raman lidar and provides volume linear depolarization-ratio profiles at 355 and 532 nm with high accuracy (Freudenthaler et al., 2016; Bravo-Aranda et al., 2016). POLIS is used as the reference polarization lidar system in EARLINET calibration and quality-assurance activities. The deployment of both lidars at the same site was motivated by the fact that the 13-channel BERTHA lidar, which integrates the HSR lidar technique, Raman aerosol, water vapor, and temperature profiling methods, and now in addition the multiwavelength depolarization-ratio profiling option in one system, **is a complex lidar system with** a large number of potential sources for uncertainties (see Appendix A). Therefore to avoid any risk and to guarantee a high-quality SALTRACE data set of multiwavelength depolarization ratio profiles, we decided to run POLIS and BERTHA side by side during the entire SALTRACE-1 campaign at CIMH.

The full overlap of the laser beams of POLIS with the RFOV is at about 200 to 250 m above ground (Groß et al., 2016), so well within the marine boundary layer (MBL) and below the lofted Saharan air layer (SAL). The range resolution of the

7

raw data is 3.75 m, the temporal resolution 5–10 s depending on atmospheric conditions. The repetition rate of the frequency doubled and tripled Nd:YAG laser is 10 Hz with a pulse energy of 50 mJ at 355 nm and 27 mJ at 532 nm (see Table 1 for more details).

2.5 CALIOP

5   Spaceborne lidar observations of the 532 nm particle linear depolarization ratio are used for comparison with the 532 nm particle depolarization ratios from the ground-based lidar observations during SAMUM-1, SAMUM-2, and SALTRACE. We analyzed all CALIOP observations (CALIPSO, 2016) for well-defined areas over Morocco (26°–31°N, 3°–8°W), in the Cabo Verde region (13°–18°N, 21°–26°W), and around Barbados (10°–15°N, 55°–60°W), performed in June 2013 (11–13 overpasses), July 2013 (15–17 overpasses), June 2014 (13–16 overpasses), and July 2014 (11–14 overpasses). We checked all day

10   and night overpasses (scenes) for the presence of dust and averaged all dusty signal profiles within the defined areas. In order to retrieve the dust depolarization ratio profiles for each overpass, only the observations characterized as dust from the CALIPSO subtype algorithm (Omar et al., 2009) are used. In these profiles, the particle linear depolarization ratio is recalculated from L2 perpendicular and total backscatter profiles, to improve the accuracy compared to the original CALIPSO L2-Version 3 product which has a known error (Tesche et al., 2013; Amiridis et al., 2013). Furthermore, several quality control procedures

15   and filtering criteria are applied in the data set as described in (Marinou et al., 2017).

In the next step, we selected those height ranges (below 6 km height) of the monthly mean profiles in which the depolarization ratios were almost height independent, and computed the column-**averaged** 532 nm particle depolarization ratio for these specific height ranges. These column values are used for comparison in Sect. 4 and 5. The selected height ranges with almost height-independent depolarization ratios extended from 800–1000 m to 3700–5600 m (above sea level, Morocco), from 1500–

20   2300 m to 4800–5400 m (Cabo Verde), and from 2500 to 3200–4200 m (Barbados). At lower heights, contamination with aerosol pollution and/or marine particles caused a significantly lower depolarization ratio. Therefore these lower heights were not considered in the dust-related depolarization data analysis.

2.6 AERONET photometers

Three sun photometers were run during the SALTRACE campaign at CIMH lidar station in 2013. Besides two CIMEL sun/sky

25   photometers of AERONET (Aerosol Robotic Network) (Holben et al., 1998) from TROPOS and the University of Valladolid (see **Barbados_SALTRACE,** AERONET (2016)), an automatic sun/sky radiometer of the Meteorological Institute of the University of Munich measured the spectral aerosol optical thickness (AOT) and sky radiances (Toledano et al., 2009, 2011). The photometers covered a wavelength range from 340–1640 nm. The TROPOS photometer was operated from June 2013 to July 2014 (with an interruption from October 2013 to February 2014 caused by a damage of the sun photometer). Another pho-

30   tometer of AERONET is installed at Ragged Point (east coast of Barbados) in the vicinity of the Barbados Cloud Observatory (Stevens et al., 2016). The Ragged Point photometer performs measurements since 2007.

2.7 Radiosonde profiling

As during the SAMUM-1 and 2 campaigns we regularly performed radiosonde observations. The Vaisala RS92 radiosondes measuring height profiles of temperature, air pressure, relative humidity, wind speed and direction up to heights above 20 km were launched around local noon (15:00–16:00 UTC, 11:00–12:00 local time) and after sunset (23:00–24:00 UTC, 19:00–20:00 local time). In total 133 radiosonde ascends were conducted at CIMH, 56, 35, and 42 during the SALTRACE-1, 2, and 3 campaigns, respectively.

3 SALTRACE case studies

Three case studies are presented to discuss the quality and accuracy of the spectrally-resolved depolarization-ratio observations with BERTHA. The first case study from summer 2013 offers the opportunity of direct comparisons with the Munich lidar system POLIS measured at the same field site in the framework of the SALTRACE-1 campaign (Groß et al., 2015). In summer 2014 only the lidar system BERTHA measured the transported Saharan dust. Two cases are shown, the first with a cirrus cloud, there the depolarization ratio is known, and the second, there the same dust reached one week later the North American continent and was measured by the HSRL-2 (Burton et al., 2015).

3.1 Case study I: Comparison of POLIS and BERTHA observations (11 July 2013)

A strong and long-lasting dust outbreak occurred from 9–13 July 2013. Figure 2 shows the BERTHA observations of the lofted SAL in the evening of 10 July 2013 (19:15–20:45 local time). The African air mass crossed Barbados with 15–20 m s^{-1} wind speed from east to west according to the radiosonde profiles (upper left panel in Fig. 2). The relative humidity ranged from 30–50% in the dust layer between 1.75 and 4.6 km height (lower left panel in Fig. 2). The moist marine aerosol layer (MAL) indicated by high relative humidity around 80–90% reached to 1.75 km height on this evening. **The marine boundary layer (MBL) is the convective part of the MAL and is often topped with trade wind cumuli. The MAL extends up to the base of the SAL which coincides with the trade wind inversion zone.** Downward mixing of dusty air into upper part of the marine aerosol layer is visible in the lower right panel in Fig. 2 (green colors between 0.5 km and 1.5 km above sea level). This layer is also called intermediate layer (Jung et al., 2013), due to its location between the convective boundary layer and the SAL. The heterogeneous structures in the 532 nm volume depolarization height-time display in Fig. 2 below 1.5 km height are caused by island effects. Differences in orography and heat release over land and ocean surfaces disturb the air mass flow in the lowest part of the atmosphere (Jähn et al., 2016). Such vertical mixing features were not observed during the SALTRACE shipborne lidar observations over the open Atlantic in May 2013 (Kanitz et al., 2013; Rittmeister et al., 2017). The backward trajectories in Fig. 3 at 3000 m height indicate dust uptake over desert areas of Northwest Africa so that contamination with anthropogenic pollution was probably low. The dusty air masses traveled 5–7 days across the Atlantic to Barbados.

Figure 4 presents the particle optical properties obtained with the **conventional Raman lidar technique (Ansmann et al., 1992).** Typical features of Saharan dust were observed **(Mattis et al., 2002; Papayannis et al., 2005; Tesche et al., 2011a;**

Preißler et al., 2011; Veselovskii et al., 2016; Hofer et al., 2017). The backscatter and extinction coefficients at 355 and 532 nm are similar and the dust 1064 nm backscatter coefficient is significantly lower than the respective 532 nm backscatter coefficient in the SAL. The observed Saharan dust lidar ratios accumulate in the 50–60 sr range at 355 and 532 nm. Below 1.75 km height a mixture of marine particles and dust particles prevailed so that the lidar ratio decreased. For pure marine condi-
5 tions, the lidar ratio would be close to 15–25 sr **(Flamant et al., 1998; Groß et al., 2011b; Burton et al., 2012; Dawson et al., 2015; Rittmeister et al., 2017; Haarig et al., 2017)**. The SAL AOT was about 0.3 at 355 and 532 nm on this day. Figure 5 shows the particle linear depolarization-ratio profiles obtained with POLIS and BERTHA on 11 July 2013, 00:00–00:45 UTC. The POLIS backscatter coefficients in the left panels of Fig. 5 are computed by applying the Klett method with a dust lidar ratio of 55 sr within the SAL and 30–40 sr below the SAL (Groß et al., 2015). The Raman lidar method is used in the computation
10 of the backscatter profiles from the BERTHA observations.

As can be seen, very good agreement is obtained regarding the volume linear depolarization ratio at 355 and 532 nm. In the computation of the particle depolarization ratio, the particle backscatter coefficients are required and cause further uncertainty. This impact is most sensitive at 355 nm. The apparent noise in the 355 nm particle depolarization ratio profiles is caused by the used backscatter coefficients. At 355 and 532 nm the SAL mean particle depolarization ratio can be compared between
15 BERTHA (0.25 and 0.28 at 355 and 532 nm respectively) and POLIS (0.26 and 0.27). Both systems agree very well. Only BERTHA measured at 1064 nm, and derived a SAL mean particle depolarization ratio of 0.22. Below the SAL, all particle depolarization ratios decrease. The down-mixed dust prevent a decrease towards pure marine values of 0.02–0.03 (Groß et al., 2011b). In the right panel of Fig. 5, profiles of the ratio of particle depolarization ratios (355 nm over 532 nm in blue, 1064 nm over 532 nm in red) are shown. The mean values are 0.81 (1064/532 nm) and 0.88 (355/532 nm). The observed height-
20 independence of the particle depolarization ratios at all three wavelengths and of the less noisy ratio of the 1064-to-532 nm depolarization ratios implies a vertically homogeneous dust size-shape characteristics. An impact of gravitational settling leading to a decrease of coarse-mode dust concentration in the SAL top region after 5–10 days of travel, which would show up in a significant change in the spectral slope of the depolarization ratio (especially at 1064 nm), is not visible. This corroborates the hypothesis proposed by Gasteiger et al. (2017) that heating of the dust particles and turbulent mixing of the SAL air masses
25 during daytime hours may widely reduces coarse-mode dust removal by gravitational settling of particles.

3.2 Case study II: Measurements of the dust layer and a cirrus (20 June 2014)

During SALTRACE-3 in 2014, POLIS was not available. Cirrus depolarization measurements were used to check the quality of triple-wavelength depolarization observations over time. Ice crystals are very large compared to the laser wavelengths so that the spectral dependence of backscattering, extinction, and depolarization properties is rather weak.
30 Figure 6 presents a cirrus measurement performed on 20-21 June 2014. The cirrus layer between 12 and 14 km height was optically thin with an AOT of 0.1. The wavelength-independent backscatter coefficients of up to 3.5 Mm^{-1} sr^{-1} at cirrus center indicate peak particle extinction values of 100-120 Mm^{-1}. The extinction values are obtained by applying a multiple-scattering-corrected cirrus lidar ratio of 30–35 sr to the cirrus backscatter coefficients (Haarig et al., 2016b). The extinction measured with the Raman channels would need a too large smoothing length in the thin cirrus.

As shown in the right panel of Fig. 6, depolarization ratios within the cirrus (above 12.2 km height) for 532 and 1064 nm are almost equal up to cloud top. The 1064 nm particle linear depolarization ratio is close to 0.5 and height-independent from 12.2–13.3 km height. The noisy 355 nm particle depolarization ratio is less trustworthy, but close to the 532 nm and 1064 nm depolarization ratios at least in the cirrus backscatter center from 12.4–12.8 km height. This consistent cirrus measurement

5 of wavelength-independent cirrus backscatter and depolarization corroborate that BERTHA was performing well and that our dust observations below 5 km height are trustworthy.

Figure 7 shows the aerosol layers in the lower troposphere on this cirrus day. A 3 km thick SAL was present above the marine aerosol layer. Relative humidities of 40–50% in the SAL were comparably high and suggest some mixing with moist marine air.

10 The HYSPLIT backward trajectories in Fig. 8 corroborate this hypothesis. 4 days before arriving at Barbados, the air masses at 2.5 km height had the chance of vertical mixing with marine particles or African pollution. Only the uppermost dust layer (3–4 km height over Barbados, trajectories not shown) seems to contain pure dust. The air masses arriving at 3.5 km height were above 6 km over desert areas in western Africa.

Figure 9 presents the particle optical properties derived from the BERTHA observations. A steady and almost monotonic

15 decrease of the backscatter coefficients with height was found. The extinction coefficients at 355 and 532 nm are again very close and the SAL AOT was about 0.25. The lidar ratios range from 40–50 sr in the layer from 1–3 km height, which probably contained some marine and anthropogenic haze particles, and was higher with values of 50–60 sr in the uppermost pure dust layer (3–4 km height).

The height profiles of the 532 and 1064 nm particle depolarization ratio show slightly different profile shapes. The 1064 nm

20 depolarization ratio decreases slightly with height whereas the 532 nm increases with height. Since the 1064 nm depolarization ratio is very sensitive to coarse-mode particles, the decrease of the 1064 nm depolarization ratio (and of the ratio of 1064-to-532 nm depolarization ratios) may be related to a decreasing coarse-mode mean radius of the particles with height. The 532 nm depolarization ratio, on the other hand, seems to be relatively insensitive against small changes in the coarse-mode size distribution (Mamouri and Ansmann, 2017). The 532 nm depolarization ratio for coarse mode particles is always in the range

25 of 0.35-0.4. The slightly lower 532 nm depolarization values around 2 km height may again indicate a different history of the dust transport. The more fine-mode sensitive depolarization ratios (355 and 532 nm) and the respective ratio of 355-to-532 nm depolarization ratios show an almost height-invariant behavior when ignoring the noise in the 355 nm depolarization ratio profile.

3.3 Case study III: Dust transport from Africa to Missouri over 12000 km (6 July 2014)

30 A unique case was observed during SALTRACE-3 on 6 July 2014. A 3 km deep dust layer crossed Barbados and traveled westward towards the United States (see backward trajectories in Fig. 10). Coincidentally, this aged dust layer was observed with an airborne triple-wavelength polarization lidar (high spectral resolution lidar HSRL-2) one week later (Burton et al., 2015). We use this unexpected opportunity to compare the triple-wavelength depolarization observations of aged dust after long-range transport over 6000 km (Barbados) and 12000 km (**Missouri**, Midwestern USA). Rather low relative humidities

around 20% were measured with radiosonde in the lofted SAL (see lower left panel in Fig. 11) suggesting almost no interference with cloud formation and associated upward mixing of marine air into the lower part of the SAL. High wind speeds around 18 m s^{-1} prevailed above 2.5 km height over Barbados. The 12.5-day backward trajectories indicate that the dust observed over Barbados at 2.5 and 3.5 km height descended towards 1.6 and 2.4 km height over **Missouri**, after crossing Yucatan (Mexico), Texas, and Oklahoma. After leaving the Africa continent, the dust layers arrived after 5 and 12 days over Barbados and **Missouri**, respectively.

Fig. 12 shows the aerosol optical properties derived from the BERTHA measurements. The triple-wavelength particle linear depolarization observations performed over **Missouri** are added. The backscatter, extinction, and lidar ratio profiles again show typical dust optical properties. The SAL AOT was about 0.3 over Barbados on this day. The backscatter and extinction coefficients were roughly 25-30% lower in the lofted dust layer over **Missouri** compared to the values measured over Barbados one week before.

An excellent agreement between the two lidar data sets of depolarization ratio profiles was found. When comparing the values in the layers from 2.5–4.0 km height over Barbados with the values in the layer from 1.5–2.0 km height over **Missouri**, both lidars found similar depolarization ratios. At 532 nm (0.28 (BERTHA) and 0.30 (HSRL-2)) and 1064 nm (0.26 (BERTHA) and 0.27-0.28 (HSRL-2)), the depolarization ratio over Barbados is slightly lower. The 355 nm depolarization ratio measured with BERTHA with a larger systematic uncertainty is around 0.24 and therefore higher than over Missouri (0.21 (HSRL-2)). But spectral behavior of the 1064 nm to the 532 nm depolarization ratio was the same over Barbados and Missouri (0.91). The 355/532 ratio of depolarization ratios decreased between Barbados and the US.

Note also, the higher depolarization ratios in the planetary boundary layer over **Missouri**. Probably new soil dust particles were injected into the continental planetary boundary layer and then mixed upward into the lofted aged SAL over the United States. This entrainment of fresh coarse dust influences especially the 1064 nm depolarization ratio. Fine-mode pollution is released as well over the United States, and upward mixing and entrainment of pollution aerosol into the SAL affects most sensitively the 355 nm depolarization ratio. Nevertheless, the agreement is surprisingly good. Even after 7 days of travel from Barbados to the Midwestern United States, the Saharan aerosol widely preserved its dust characteristics. No significant height-dependence of the optical properties (lidar ratio, depolarization ratio, ratio of depolarization ratios) is visible in the main parts of the layer over both sites.

4   SALTRACE statistical overview

Figure 13 provides an overview of all triple-wavelength depolarization-ratio observations with BERTHA during the summer SALTRACE campaigns. SAL mean values of 8 evening sessions (SALTRACE-1, summer 2013) and 13 evening session (SALTRACE-3, summer 2014) are shown. The respective mean values derived from the BERTHA observations in June 2013 and 2014 and July 2013 and 2014 are shown as horizontal lines. In addition, monthly means of the SAL column dust depolarization ratio obtained from spaceborne lidar CALIOP observations at 532 nm in the Barbados region are presented.

12

The number of evening observations with a complete set of depolarization ratios at all three wavelengths is comparably low for SALTRACE-1 (2013) because of many days with rainy and cloudy weather, days without dust, and also due to problems with one of the lasers. In 2014, 13 evening data sets of triple-wavelength depolarization ratio profiles out of a total of 21 possible evening lidar sessions could be used for the statistics in Fig. 13. Less days with closed cloud decks and rain periods **hampered**

5   observations in 2014. The five-week SALTRACE-1 field phase was embedded in a typical tropical wet season. Short-term dust episodes were frequently interrupted by rainy weather. Radiosonde profiles often showed different wind directions from south to northeast within the 3–5 km thick Saharan dust layers until 9–10 July 2013. Cloud formation and activation of dust particles to serve as cloud condensation nuclei, rain and corresponding washout probably significantly influenced the dust characteristics during the long-range transport across the Atlantic. A pronounced, well-defined dust outbreak lasting over several days was

10   observed from **9–13** July only during the SALTRACE-1 campaign in 2013. Most of the July 2013 observations in Fig. 13 were taken during this final SALTRACE-1 dust outbreak. In contrast, more homogeneous, vertically well-structured dust outbreaks were observed in June and July 2014. The summer of 2014 was an extraordinary dry season in the Barbados area and over the tropical Atlantic. Cloud processing and washout by rain was strongly suppressed in the summer of 2014. **Continuous and almost undisturbed dust transport from Africa towards the Caribbean occurred.**

15   The fluctuations in the individual depolarization ratio values in Fig. 13 partly reflect the impact of cloudy and rainy weather. The mean values (horizontal lines) for July 2013 (with the well-defined dust outbreak), June and July 2014 differ significantly from the ones for June 2013 for the wavelengths of 532 and 1064 nm. On average, the 532 and 1064 nm particle depolarization ratios accumulated in the **0.28–0.30** and 0.22–0.26 range, respectively, during the more dry and less cloud and rain-affected periods. A similar contrast (wet 2013 vs dry 2014 months) is observed with CALIOP. The CALIOP monthly means include

20   SAL column values around Barbados (**10°–15° N, 55°–60° W**). The large standard deviation bars of the CALIOP monthly means in Fig. 13 mainly indicate the atmospheric variability within the defined areas given in Sect. 2.5. Good agreement between the BERTHA and the CALIOP measurements is found.

A considerable part of the scatter in the BERTHA data is however caused by retrieval uncertainties (see the systematic uncertainty bars in Fig. 13). These uncertainties are rather large for 355 nm. The error bars of the individual measurements

25   only show the variability (standard deviation, SD) around the mean values within the observed individual SAL height range from base to top. The systematic errors of the 1064 nm particle depolarization ratio are comparably small. Thus the fluctuations of the 1064 nm depolarization ratio **indicate** the changes in the dust microphysical characteristics from day to day. **The large-particle fraction is expected to vary with time as a function of varying dust removal strength due to different travel conditions across the Atlantic and different weather conditions. This especially influences the 1064 nm SAL mean**

30   **depolarization ratio according the discussion below. The depolarization ratio measurements at 1064 nm will improve the retrieval of microphysical properties according to Gasteiger and Freudenthaler (2014).**

Table 2 provides the overall SALTRACE (summers of 2013 and 2014) mean depolarization ratio values for all three wavelengths, the associated SD values (**showing the day-to-day variability of the SAL**), and typical systematic retrieval errors. Typical systematic errors are obtained from averaging of the respective uncertainties of the 21 evening observational cases.

35   The SALTRACE mean depolarization ratios are 0.25 (355 nm), **0.28** (532 nm), and 0.23 (1064 nm).

We found good agreement between the two depolarization data sets collected with POLIS (Groß et al., 2015) and BERTHA for July 2013. On average, particle depolarization ratios were 0.28 (POLIS) and 0.29 (BERTHA) at 532 nm and 0.27 (POLIS) and 0.26 (BERTHA) at 355 nm. For June 2013, the results at 532 nm differ significantly. On average, we observed with BERTHA June 2013 means of 0.26 (532 nm) and 0.26 (355 nm) based on four individual evening measurements. The POLIS June 2013 mean values (based on three evening measurement sessions) were higher at 532 nm (0.29) and equal at 355 nm (0.26). The large systematic uncertainties in the BERTHA depolarization ratios are probably mainly responsible for the observed differences as well as the low number of observations which is too low for drawing solid conclusions on the quality of the measurements.

5 Discussion

Figure 14 provides an overview of the entire SAMUM-SALTRACE data set of depolarization ratios collected from 2006 to 2014 in southeastern Morocco (SAMUM-1), at Praia, Cabo Verde (SAMUM-2), and on Barbados (SALTRACE). There is almost no change of the mean 355 nm and 532 nm particle depolarization ratio with distance from the dust source when combining the BERTHA (Barbados) and POLIS/MULIS (Cabo Verde, Morroco) data sets. The POLIS/MULIS data sets indicate a slow decrease of the mean 532 nm depolarization value from 0.31 (Morocco) over 0.30 (Cabo Verde) toward 0.28 (Barbados), **but the difference is not significant**. The available 1064 nm mean values indicate a significant decrease from a Morocco mean value of 0.27 to a Barbados mean value of 0.23. We speculate that a large fraction of large dust particles causing depolarization ratios of 0.40 is present over areas close to the Sahara but that these large particles are widely removed before reaching Barbados. The other two wavelengths (355 and 532 nm) are more sensitive to fine-mode dust (accumulation-mode particles with diameters <1 μm), for which the removal by gravitational settling is less efficient. Especially, the 355 nm SAL values, widely controlled by fine-mode dust particle, show a rather robust behavior. No trend in the 355 nm depolarization values is observed in the SAMUM-1, 2 and SALTRACE data.

Figure 14 includes CALIOP depolarization measurements performed in the Morocco, Cabo Verde, and Barbados region in June and July of 2013 and 2014. The overall four-month mean values (plus SD) are shown. The CALIOP 532 nm mean values (and SD) are 0.31±0.07 (Morocco), **0.30±0.05** (Cabo Verde), and **0.30±0.06** (Barbados). Good agreement between the ground-based BERTHA and spaceborne CALIOP observations is obtained, and no significant trend in the 532 nm particle depolarization ratio found. Veselovskii et al. (2016) reported an average 532 nm particle linear depolarization ratios of 0.30±0.045 for the SHADOW campaign in Senegal during dust outbreaks in March-April 2015.

The found spectral slope of the depolarization ratio, **shown in Fig. 15,** with the maximum at 532 nm and lower values at 355 and 1064 nm reflects the different influence of the fine-mode and coarse-mode dust fractions on the overall (fine + coarse) particle depolarization ratio at the three wavelengths. The 355 nm dust particle depolarization ratio is strongly influenced by fine-mode dust (up to 50–60% fine mode fraction (FMF) according to AERONET observations). Fine-mode dust causes a depolarization ratio around 0.20 at 355 nm. The comparably weak influence of coarse-mode dust (causing depolarization ratios >0.30) leads to an overall (fine + coarse-mode) particle linear depolarization ratio of 0.25±0.03. The

532 nm dust depolarization ratio is still sensitively influenced by fine-mode dust (FMF 10–30% contribution, causing a fine-mode depolarization ratio around 0.15) but also by the coarse-mode dust particle fraction (leading to a depolarization ratio of 0.35–0.40). The overall effect of fine-mode and coarse-mode depolarization then leads to the observed 532 nm depolarization ratios around 0.30±0.03. In contrast, the 1064 nm dust particle depolarization ratio is caused to about 95% by coarse-mode dust particles (FMF 5%) according to AERONET observations, and seems to be between 0.20–0.28 for dust after long-range transport. The influence of the fine and coarse-mode dust fractions on the particle linear depolarization ratio is discussed in detail by Mamouri and Ansmann (2017).

Simulation studies of Kemppinen et al. (2015a) can be used to interpret our depolarization observations. These simulations are based on realistic dust particle shapes, measured during SAMUM-1 in Morocco (Lindqvist et al., 2014). For the so-called dolomite shape type, the simulations yield 1064 nm and 532 nm coarse-mode particle linear depolarization ratios of 0.20–0.25 and 0.35–0.40, respectively, provided dust particles with diameters around 2 μm dominate backscattering of laser photons. These depolarization values are in good agreement with the 1064 nm lidar observations as well as with 532 nm depolarization studies when taking a dust fine-mode fraction of 20% (as indicated by AERONET sun photometer observations), a fine-mode depolarization ratio of 0.15, and a measured 532 nm depolarization ratio of 0.30 into account, as explained in detail by Mamouri and Ansmann (2017). It is interesting to note in this context that the AERONET photometer observations during dust outbreaks over Barbados in 2013 and 2014 show that the coarse-mode effective diameter accumulates around 3±0.4μm which indicates that most coarse-mode dust particles after long-range transport have diameters in the 1-3 μm size range. Veselovskii et al. (2016) retrieved overall (fine-mode + coarse-mode) effective diameters of 2–2.5 μm from the multi-wavelength lidar measurements in the dust plumes over Senegal during the SHADOW campaign.

This consistency between the lidar observations, photometer retrievals and simulation studies is promising and suggest that our triple-wavelength polarization lidar observations are very useful for next steps in dust simulation studies with the goal to develop an appropriate dust size-shape parametrization scheme for atmospheric weather and climate models. However, the consistency created here is not more than an hypothesis. Much more laboratory and model studies together with our complex field observations are required to improve stepwise our knowledge on the complex relationship between fundamental dust properties and related optical effects.

Figure 15 provides a comparison of the observations with triple-wavelength polarization lidars (BERTHA, HSRL-2) and a **preliminary modeling result** of the depolarization ratios described by Gasteiger et al. (2017) in their hypothesis with vertical mixing during the day. A mix of irregularly shaped (non-spheroidal) particles and small spherical ammonium sulfate particles is assumed in the simulation. The mineralogical variability is mimicked by mixing of absorbing and non-absorbing particles. The spectral trend observed with the lidars is also visible in the simulation. **The deviation of the modeled spectral slope of the depolarization ratio from the observed wavelength dependence may be related to the shape parametrization of the rough estimate of the dust size distribution. Fig. 15 may be regarded as the starting point of a comprehensive modeling effort.** A dense observational data on depolarization ratios together with airborne in situ observations of size distributions and the mineralogical/chemical composition of the dust particles in the Barbados region (Weinzierl et al., 2017) is now available for in-depth simulation studies of dust optical properties.

6 Conclusions

Triple-wavelength polarization lidar measurements in **long-range transported** Saharan dust layers were performed at Barbados, 5000–8000 km west of the Saharan dust sources, in the framework of three SALTRACE campaigns, each lasting over several weeks. High quality was achieved by comparing the BERTHA observations with depolarization ratio profiles measured with a reference system and by using cirrus layers in which the spectral dependence of the particle depolarization ratio vanishes. A unique case of long-range transported dust over more than 12000 km was presented and indicated widely unchanged Saharan dust optical properties even after a travel time of two weeks since the emission. On average, the particle linear depolarization ratios for aged Saharan dust were found to be **0.252±0.030 at 355 nm, 0.280±0.020 at 532 nm, and 0.225±0.022 at 1064 nm (mean ± standard deviation)**. According to published simulation studies we conclude that most of the coarse-mode dust particles have sizes around 2 μm in diameter after one week of travel. By comparing the SALTRACE results to the SAMUM-1 and SAMUM-2 results, again, only minor changes in the dust depolarization characteristics were observed on the way from the Saharan dust sources towards the Caribbean. **Only the 1064 nm depolarization ratio mean value decreased significantly from Morocco towards the Caribbean.**

A long-term data set of the particle linear depolarization ratio of mineral dust measured simultaneously at 355, 532, and 1064 nm is now available. In addition, dense 355 and 532 nm lidar ratio data sets are available (Groß et al., 2011a, 2015; Tesche et al., 2011a). Furthermore, airborne in situ observations of the dust particle size distribution and chemical composition in the SAL are available (Weinzierl et al., 2017). This is an excellent basis for comprehensive simulation efforts to develop realistic dust shape models and parametrization schemes which link the dust size distribution, composition, and shape characteristics with the resulting optical and radiative properties of mineral dust particles.

The available coherent multiwavelength data sets on linear depolarization ratios and lidar ratios (from the source region to remote areas of long-range transport) support present and upcoming spaceborne lidar missions (CALIPSO and EarthCARE missions) and the development of new space lidar mission concepts (based on multiwavelength polarization/HSRL lidar missions). They can further be used to harmonize existing and future depolarization data sets collected at different lidar wavelengths. Furthermore, existing dust retrieval schemes such as the technique presented in this SALTRACE special issue by Mamouri and Ansmann (2017) can be checked and improved based on the available complex depolarization ratio data sets.

Together with the observations of the 355 and 532 nm depolarization ratios with POLIS (EARLINET reference system) a high quality data set on depolarization ratios at 355, 532, and 1064 nm for Saharan dust after long range transport is now available for the first time. Comparison with another triple-wavelength depolarization ratio data set indicates that the Barbados data is very trustworthy. CALIOP depolarization ratios collected over the SAMUM-1, SAMUM-2, and the SALTRACE field sites are in very good agreement with the findings of the ground-based lidars. Altogether, a significant dust aging effect triggering a significant change of the dust depolarization ratio from regions close to the source to areas more than 5000 km downwind is not visible in the observations. Discrepancies between the modeled and the observed depolarization ratios are not surprising when keeping in consideration that the shape characteristics of the irregularly shaped dust particles is not well known, and a realistic shape model is not existing.

16

As an outlook, we are presently testing to measure besides dust depolarization ratios at three wavelengths also the dust extinction coefficient at these three wavelengths. First test observations were promising (Haarig et al., 2016b).

7 Data availability

HYSPLIT backward trajectories are calculated via the available simulation tools (HYSPLIT, 2016). AERONET sun photometer AOT data are downloaded from the AERONET web page (AERONET, 2016). SALTRACE BERTHA lidar data are available at TROPOS. CALIOP signal profile data are made available by the CALIPSO science team (CALIPSO, 2016). We used level 2 version 3.30 CALIPSO Aerosol profile data.

Appendix A: Polarization channels and their calibration in the lidar system BERTHA

The appendix A explains shortly the state of the art concept of polarization lidar according to Freudenthaler (2016) and discusses some special features of the BERTHA lidar system. In the second part, the BERTHA lidar system will be characterized in detail and the systematic errors will be estimated.

5

A1   Calculation of the depolarization

In a state-of-the-art approach the components of the lidar system are described by Mueller matrices using the Mueller-Stokes formalism (Freudenthaler, 2016):

$$\boldsymbol{I}_\mathrm{S} = \eta_\mathrm{S}\mathbf{M}_\mathrm{S}(D_\mathrm{S}, \nu_\mathrm{S}, \Delta_\mathrm{S})\mathbf{C}(\Psi, \epsilon)\mathbf{M}_0(D_0, \gamma, \Delta_0, a_0)\mathbf{F}(a)\mathbf{M}_\mathrm{E}(D_\mathrm{E}, \beta, \Delta_\mathrm{E}, a_\mathrm{BE})\boldsymbol{I}_\mathrm{L}(\alpha) \tag{A1}$$

10 The different quantities have to be known or at least good estimates and their uncertainties are needed. They will be described in the following text and determined for each wavelength separately in the next section. An overview is given in Table 3.

All the rotational misalignment around the optical axis (rotational misalignment in the following) is with respect to the plane of polarization of the polarization filter in front of the PMT belonging to the cross polarized channel of the corresponding wavelength. The emitted laser light $\boldsymbol{I}_\mathrm{L}$ is has a rotational misalignment α.

15 The emitting optics $\mathbf{M}_\mathrm{E}$ (beam expander and steering mirrors) have a diattenuation parameter (called diattenuation in the following) D_E, a retardation Δ_E and a misalignment β. Furthermore the beam expander may cause depolarization due to inhomogeneities over its surface and birefringence of the calcium fluoride lens. The degree of linear polarization after the beam expander is given by a_BE.

$\mathbf{F}$ represents the scattering process in the atmosphere with an atmospheric polarization parameter a corresponding to the

20 atmospheric **volume linear depolarization ratio** δ:

$$a = \frac{1-\delta}{1+\delta} \tag{A2}$$

which is the unknown quantity, that will be derived by polarization lidar measurements.

The receiving optics $\mathbf{M}_0$, in the case of BERTHA only the telescope and a 90° mirror, are characterized by the diattenuation D_0, the retardation Δ_0 and the misalignment γ.

25 A linear polarizer is used for the calibration C, the position Ψ is +45° or -45° and ϵ is the deviation of this ideal position, but not affecting the exact 90° angle between the two calibration positions (±45°). The exact difference is reached by a highly accurate (10^{-4} degrees) step motor (8SMC1 from Standa Ltd., Lithuania). The calibrator is only used during the calibration measurements. For the regular measurements, it is taken out of the beam and therefore a possible misalignment is not affecting the measurements.

30

The detection units for the total channel (index S=T) and for the cross polarized channel (index S=R), $\mathbf{M}_\mathrm{T}$ and $\mathbf{M}_\mathrm{R}$, include a diattenuation, which would be ideally $D_\mathrm{T}=0$ and $D_\mathrm{R}=-1$. **In addition** to Freudenthaler (2016) a rotational misalignment ν_S

and a retardation Δ_S has to be included in the formulas for the BERTHA lidar system. **The calibrator is located behind the telescope and before the beam separation unit** (see Fig. 1). The retardation Δ_S has no effect on the measured intensity and need no further consideration. For the total channel there is no rotational misalignment, only ν_S for the cross polarized channel has to be taken into account. The gain ratio of the PMT and its neutral density filters is represented by η_T and η_R, respectively.

5 A calibration measurement for every change in the neutral density filters was performed.

Freudenthaler (2016) presents a solution to the matrix equation (eq. A1) introducing the parameters G_S and H_S as system constants. They are a simplification in the notation of the solution and depend on all previous mentioned system parameters (Tab. 3). The remaining unknown is the atmospheric polarization parameter a. The intensity (first component of the Stokes vector $\boldsymbol{I}_S$) is given by:

10 $$I_S = \eta_S T_S T_0 F_{11} T_E I_L \left(G_S + a H_S \right) \tag{A3}$$

with the laser intensity I_L, the transmittance of the emitting optics T_E, of the receiving optics T_0, of the detection unit T_S, the backscatter coefficient F_{11} and the gain of the detector η_S. Taking the ratio of two signals, only T_S and η_S are remaining. The volume linear depolarization ratio δ_v can be determined:

$$\delta_v = \frac{\delta^*(G_T + H_T) - (G_R + H_R)}{(G_R - H_R) - \delta^*(G_T - H_T)} \tag{A4}$$

15 with the calibrated signal ratio δ^*:

$$\delta^* = \frac{1}{\eta} \frac{I_R}{I_T} \tag{A5}$$

with calibration factor η, determined by the $\Delta 90°$-calibration (Freudenthaler et al., 2009). The measured calibration factor η^* has to be corrected for any of the above mentioned rotational misalignment. The correction constant K is used to obtain the calibration factor η (Freudenthaler, 2016):

20 $$\eta = \frac{\eta^*}{K} \tag{A6}$$

The five parameters G_T, H_T, G_R, H_R and K (system constants) are calculated from the system characteristics (Tab. 3) for each wavelength.

A2 System characterization

The results of the system characterization are shown in Table 3. Similar characterizations of different EARLINET lidars have
25 been reported by Bravo-Aranda et al. (2016). The results are shown for the conditions during SALTRACE-3 as it has been characterized when the system was back in Leipzig. Some characterization and optimization efforts have already been done at the field site on Barbados. One year in the tropical region and the transport might influence the system performance.

The degree of linear polarization of the laser is high (>95% according to manufacturer's specification) and it is additionally cleaned by a Glen-Taylor polarizer, whose misalignment with respect to the optical table is characterized by the angle α and
30 measured with the help of an additional polarization filter with the uncertainty of 0.2°.

The beam expander is the major source of uncertainty in the emitter optics, as it has to deal with the three wavelengths simultaneously and the high power of the laser. The used CaFl lens appears to be birefringent. In order to check this issue, the beam expander was tested in the EARLINET lidar calibration center in Bucharest (www.lical.inoe.ro). The Mueller matrix elements have been measured with transmission ellipsometry at 25 points over the surface of the beam expander. Inhomogeneities of the Mueller matrix elements in the external regions of the beam expander have been found, especially in the UV. As a first approximation a degree of linear polarization of 0.97 ± 0.02 in the UV after the beam expander is assumed. In the visible and near infrared the degree of linear polarization is almost ideal (0.99 to 1.00). The influence of the other components (mainly steering mirrors) of the emitter optics is neglected so far, although the diattenuation of the emitter optics is mainly induced by these steering mirrors. From the transmission ellipsometry of the beam expander a diattenuation (D_E) smaller than 0.05 is derived. Not all elements of the Mueller matrix of the beam expander could be measured. Therefore the retardation Δ_E of the emitter optics is not known, **and the maximum uncertainty of $\pm 180°$ is assumed**. The same assumption has been made for other EARLINET lidars by Bravo-Aranda et al. (2016). An appropriate assumption for the rotational misalignment β is $0° \pm 1.0°$.

The receiver diattenuation (D_0, D_T, D_R) was characterized using an additional light source with known state of polarization ($0°$ to $360°$ in steps of $1°$) similar to Mattis et al. (2009). A second calibration measurement was performed with the internal linear polarizer after the telescope to separate the influence of D_0 from D_T and D_R. **The two calibrations indicated a depolarization of the 90°-mirror after the secondary mirror (see Fig. 1). The polarization parameter a_0 of this mirror has a significant influence at 532 nm only (a_0=0.958). For the UV (a_0>0.994) and the near infrared (a_0>0.994) it can be attributed to uncertainties in the measurement (± 0.005) and its influence is thus neglected, but considered in the error estimation.** The rotational misalignment γ of the receiving optics is assumed to be $0° \pm 0.2°$. It is a fixed, well-aligned system. The retardation of the receiver could not be measured, which lead to the maximum uncertainty of $\pm 180°$. The rotational misalignment (ν_R) in the cross polarized channel after the calibrator is assumed to be $0° \pm 0.5°$.

The deviation of the ideal calibration position ϵ can be estimated according to Freudenthaler (2016) and is only present during calibration measurements, while at the normal measurements the linear polarizer is taken out of optical path. It varies between $-3.1°$ and $1.8°$ at 355 nm, $-2.4°$ and $1.5°$ at 532 nm and $-1.1°$ and $2.4°$ at 1064 nm. The parameter K corrects the calibration constant for the misalignment ϵ. For each calibration the parameter K was calculated using the estimated ϵ. The corrections are small as $|\epsilon|<5°$.

K is mainly influenced by the contrast ratio (=1/extinction ratio) of the linear polarizer used for the calibration. The manufacturer CODIXX specifies the contrast ratio to be 1:10,000 (at 355 nm), 1:60,000 (at 532 nm) and 1:90,000 (at 1064 nm).

The 12 parameters listed in Table 3 introduce an uncertainty of the volume linear depolarization ratio. It is too complex to perform classical error propagation. Therefore a Monte-Carlo simulation is used as proposed by Bravo-Aranda et al. (2016). This is actually a complete search over the multi-dimensional uncertainty space, there the 12 parameters are varied within their error margins. Uniform distributions are used as input. The rotational misalignment ($\alpha, \beta, \gamma, \nu_R$) has been simulated with three input values $x_i - \Delta x_i$, x_i, $x_i + \Delta x_i$. The diattenuation (D_E, D_0, D_T, D_R) has been simulated with five input values $x_i - \Delta x_i$, $x_i - 0.5\Delta x_i$, x_i, $x_i + 0.5\Delta x_i$, $x_i + \Delta x_i$ as it is a are more sensitive parameter (Bravo-Aranda et al., 2016). The unknown

retardation (Δ_E and Δ_0) is simulated using 5 values as well: -180°, -90°, 0°, 90° and 180°. **The polarization parameter of the 90°-mirror in the telescope a_0 has been simulated with three values, for 355 and 1064 nm 1.000, 0.995 and 0.990 were used.** The degree of linear polarization after the beam expander a_{BE} has been simulated with three values for 532 nm and 1064 nm (1.000, 0.995 and 0.990) and 5 values for 355 between 0.95 and 0.99 in steps of 0.01. The variation of ϵ, which does not influence the calculation of G_S and H_S, has not been taken into account to reduce the number of variables by a factor of 3. In the Monte-Carlo simulation over **11** million combinations are used for 532 nm and 1064 nm. For 355 nm over **18** million combinations are used as input. The **original code, based on Freudenthaler (2016), without our modifications as mentioned above,** can be found on https://bitbucket.org/iannis_b/ (last **accessed** Feb. 2017).

The simulation has been performed for the theoretical Rayleigh values (0.0080, 0.0053, 0.0036), and typical values within the dust layer (0.08, 0.20, 0.23) for 355 nm, 532 nm and 1064 nm, respectively. For an input value (true value) the program simulates the calibrated signal ratio δ^* varying all lidar parameters within their error margins as described above. Then it calculates the volume depolarization ratio δ_v according to equation A4. The frequency distributions of the solutions are shown in Fig. 16. The minimum and maximum value as well as the standard deviation from the corresponding Gaussian distribution is summarized in Table 4.

The standard deviation is the measure for the systematic error of the volume linear depolarization. It is slightly higher in the dust layer than in the aerosol-free Rayleigh background.

The systematic error for the particle linear depolarization ratio mainly includes the uncertainties of the volume depolarization ratio (Table 4) and the backscatter ratio (molecular backscatter coefficient divided by particle backscatter coefficient). For the particle backscatter coefficient an uncertainty of 5%, 10% and 15% for 355, 532 and 1064 nm, respectively, is assumed. Less Rayleigh signal towards higher wavelengths increases the uncertainty in the reference value for the calculation of the particle backscatter coefficient. The uncertainty of the molecular backscatter coefficient is <1% because it is calculated from the temperature and pressure profiles of the radiosondes which were launched twice a day at the time of the measurements. The molecular depolarization δ_m is calculated from the transmission curves of the interference filters and depends on temperature **(Behrendt and Nakamura, 2002)**. An error of 10% is assumed.

References

AERONET: Aerosol Robotic Network aerosol data base, https://aeronet.gsfc.nasa.gov/, 2016.

Althausen, D., Müller, D., Ansmann, A., Wandinger, U., Hube, H., Clauder, E., and Zörner, S.: Scanning 6-Wavelength 11-Channel Aerosol Lidar, Journal of Atmospheric and Oceanic Technology, 17, 1469–1482, doi:10.1175/1520-0426(2000)017<1469:SWCAL>2.0.CO;2, 2000.

Amiridis, V., Wandinger, U., Marinou, E., Giannakaki, E., Tsekeri, A., Basart, S., Kazadzis, S., Gkikas, A., Taylor, M., Baldasano, J., and Ansmann, A.: Optimizing CALIPSO Saharan dust retrievals, Atmospheric Chemistry and Physics, 13, 12089–12106, doi:10.5194/acp-13-12089-2013, 2013.

Ansmann, A., Wandinger, U., Riebesell, M., Weitkamp, C., and Michaelis, W.: Independent measurement of extinction and backscatter profiles in cirrus clouds by using a combined Raman elastic-backscatter lidar, Appl. Opt., 31, 7113–7131, doi:10.1364/AO.31.007113, 1992.

Ansmann, A., Wagner, F., Müller, D., Althausen, D., Herber, A., von Hoyningen-Huene, W., and Wandinger, U.: European pollution outbreaks during ACE 2: Optical particle properties inferred from multiwavelength lidar and star-Sun photometry, Journal of Geophysical Research: Atmospheres, 107, AAC 8–1–AAC 8–14, doi:10.1029/2001JD001109, http://dx.doi.org/10.1029/2001JD001109, 2002.

Ansmann, A., Bösenberg, J., Chaikovsky, A., Comerón, A., Eckhardt, S., Eixmann, R., Freudenthaler, V., Ginoux, P., Komguem, L., Linné, H., Márquez, M. A. L., Matthias, V., Mattis, I., Mitev, V., Müller, D., Music, S., Nickovic, S., Pelon, J., Sauvage, L., Sobolewsky, P., Srivastava, M. K., Stohl, A., Torres, O., Vaughan, G., Wandinger, U., and Wiegner, M.: Long-range transport of Saharan dust to northern Europe: The 11–16 October 2001 outbreak observed with EARLINET, Journal of Geophysical Research: Atmospheres, 108, n/a–n/a, doi:10.1029/2003JD003757, http://dx.doi.org/10.1029/2003JD003757, 4783, 2003.

Ansmann, A., Tesche, M., Knippertz, P., Bierwirth, E., Althausen, D., Müller, D., and Schulz, O.: Vertical profiling of convective dust plumes in southern Morocco during SAMUM, Tellus B, 61, 340–353, doi:10.1111/j.1600-0889.2008.00384.x, 2009.

Ansmann, A., Petzold, A., Kandler, K., Tegen, I., Wendisch, M., Müller, D., Weinzierl, B., Müller, T., and Heintzenberg, J.: Saharan Mineral Dust Experiments SAMUM–1 and SAMUM–2: what have we learned?, Tellus B, 63, 403–429, doi:10.1111/j.1600-0889.2011.00555.x, 2011.

Ansmann, A., Rittmeister, F., Engelmann, R., Basart, S., Benedetti, A., Spyrou, C., Skupin, A., Baars, H., Seifert, P., Senf, F., and Kanitz, T.: Profiling of Saharan dust from the Caribbean to West Africa, Part 2: Shipborne lidar measurements versus forecasts, Atmospheric Chemistry and Physics Discussions, 2017, 1–30, doi:10.5194/acp-2017-502, http://www.atmos-chem-phys-discuss.net/acp-2017-502/, 2017.

Baars, H., Ansmann, A., Althausen, D., Engelmann, R., Artaxo, P., Pauliquevis, T., and Souza, R.: Further evidence for significant smoke transport from Africa to Amazonia, Geophysical Research Letters, 38, n/a–n/a, doi:10.1029/2011GL049200, http://dx.doi.org/10.1029/2011GL049200, l20802, 2011.

Behrendt, A. and Nakamura, T.: Calculation of the calibration constant of polarization lidar and its dependency on atmospheric temperature, Opt. Express, 10, 805–817, doi:10.1364/OE.10.000805, http://www.opticsexpress.org/abstract.cfm?URI=oe-10-16-805, 2002.

Biele, J., Beyerle, G., and Baumgarten, G.: Polarization lidar: Corrections of instrumental effects, Opt. Express, 7, 427–435, doi:10.1364/OE.7.000427, http://www.opticsexpress.org/abstract.cfm?URI=oe-7-12-427, 2000.

Bovchaliuk, V., Goloub, P., Podvin, T., Veselovskii, I., Tanre, D., Chaikovsky, A., Dubovik, O., Mortier, A., Lopatin, A., Korenskiy, M., and Victori, S.: Comparison of aerosol properties retrieved using GARRLiC, LIRIC, and Raman algorithms applied to multi-

wavelength lidar and sun/sky-photometer data, Atmospheric Measurement Techniques, 9, 3391–3405, doi:10.5194/amt-9-3391-2016, http://www.atmos-meas-tech.net/9/3391/2016/, 2016.

Bravo-Aranda, J. A., Belegante, L., Freudenthaler, V., Alados-Arboledas, L., Nicolae, D., Granados-Muñoz, M. J., Guerrero-Rascado, J. L., Amodeo, A., D'Amico, G., Engelmann, R., Pappalardo, G., Kokkalis, P., Mamouri, R., Papayannis, A., Navas-Guzmán, F., Olmo, F. J., Wandinger, U., Amato, F., and Haeffelin, M.: Assessment of lidar depolarization uncertainty by means of a polarimetric lidar simulator, Atmospheric Measurement Techniques, 9, 4935–4953, doi:10.5194/amt-9-4935-2016, 2016.

Burton, S. P., Ferrare, R. A., Hostetler, C. A., Hair, J. W., Rogers, R. R., Obland, M. D., Butler, C. F., Cook, A. L., Harper, D. B., and Froyd, K. D.: Aerosol classification using airborne High Spectral Resolution Lidar measurements – methodology and examples, Atmospheric Measurement Techniques, 5, 73–98, doi:10.5194/amt-5-73-2012, 2012.

Burton, S. P., Hair, J. W., Kahnert, M., Ferrare, R. A., Hostetler, C. A., Cook, A. L., Harper, D. B., Berkoff, T. A., Seaman, S. T., Collins, J. E., Fenn, M. A., and Rogers, R. R.: Observations of the spectral dependence of linear particle depolarization ratio of aerosols using NASA Langley airborne High Spectral Resolution Lidar, Atmospheric Chemistry and Physics, 15, 13 453–13 473, doi:10.5194/acp-15-13453-2015, 2015.

CALIPSO: CALIPSO/CALIOP Level 2, Lidar Aerosol Profile Data, version 3.30, doi:10.5067/CALIOP/CALIPSO/CAL_LID_L2_05kmAPro-Prov-V3-30_, 2016.

Chaikovsky, A., Dubovik, O., Holben, B., Bril, A., Goloub, P., Tanré, D., Pappalardo, G., Wandinger, U., Chaikovskaya, L., Denisov, S., Grudo, J., Lopatin, A., Karol, Y., Lapyonok, T., Amiridis, V., Ansmann, A., Apituley, A., Alados-Arboledas, L., Binietoglou, I., Boselli, A., D'Amico, G., Freudenthaler, V., Giles, D., Granados-Muñoz, M. J., Kokkalis, P., Nicolae, D., Oshchepkov, S., Papayan-nis, A., Perrone, M. R., Pietruczuk, A., Rocadenbosch, F., Sicard, M., Slutsker, I., Talianu, C., DeTomasi, F., Tsekeri, A., Wagner, J., and Wang, X.: Lidar-Radiometer Inversion Code (LIRIC) for the retrieval of vertical aerosol properties from combined lidar/radiometer data: development and distribution in EARLINET, Atmospheric Measurement Techniques, 9, 1181–1205, doi:10.5194/amt-9-1181-2016, http://www.atmos-meas-tech.net/9/1181/2016/, 2016.

Chouza, F., Reitebuch, O., Groß, S., Rahm, S., Freudenthaler, V., Toledano, C., and Weinzierl, B.: Retrieval of aerosol backscat-ter and extinction from airborne coherent Doppler wind lidar measurements, Atmospheric Measurement Techniques, 8, 2909–2926, doi:10.5194/amt-8-2909-2015, https://www.atmos-meas-tech.net/8/2909/2015/, 2015.

Chouza, F., Reitebuch, O., Benedetti, A., and Weinzierl, B.: Saharan dust long-range transport across the Atlantic studied by an airborne Doppler wind lidar and the MACC model, Atmospheric Chemistry and Physics, 16, 11 581–11 600, doi:10.5194/acp-16-11581-2016, http://www.atmos-chem-phys.net/16/11581/2016/, 2016a.

Chouza, F., Reitebuch, O., Jähn, M., Rahm, S., and Weinzierl, B.: Vertical wind retrieved by airborne lidar and analysis of island induced gravity waves in combination with numerical models and in situ particle measurements, Atmospheric Chemistry and Physics, 16, 4675–4692, doi:10.5194/acp-16-4675-2016, http://www.atmos-chem-phys.net/16/4675/2016/, 2016b.

Colarco, P. R., Toon, O. B., Reid, J. S., Livingston, J. M., Russell, P. B., Redemann, J., Schmid, B., Maring, H. B., Savoie, D., Welton, E. J., Campbell, J. R., Holben, B. N., and Levy, R.: Saharan dust transport to the Caribbean during PRIDE: 2. Transport, vertical profiles, and deposition in simulations of in situ and remote sensing observations, Journal of Geophysical Research: Atmospheres, 108, n/a–n/a, doi:10.1029/2002JD002659, http://dx.doi.org/10.1029/2002JD002659, 8590, 2003.

23

Curtis, D. B., Meland, B., Aycibin, M., Arnold, N. P., Grassian, V. H., Young, M. A., and Kleiber, P. D.: A laboratory investigation of light scattering from representative components of mineral dust aerosol at a wavelength of 550 nm, Journal of Geophysical Research: Atmospheres, 113, n/a–n/a, doi:10.1029/2007JD009387, http://dx.doi.org/10.1029/2007JD009387, d08210, 2008.

David, G., Thomas, B., Nousiainen, T., Miffre, A., and Rairoux, P.: Retrieving simulated volcanic, desert dust and sea-salt particle properties from two/three-component particle mixtures using UV-VIS polarization lidar and T matrix, Atmospheric Chemistry and Physics, 13, 6757–6776, doi:10.5194/acp-13-6757-2013, 2013.

Dawson, K. W., Meskhidze, N., Josset, D., and Gassó, S.: Spaceborne observations of the lidar ratio of marine aerosols, Atmospheric Chemistry and Physics, 15, 3241–3255, doi:10.5194/acp-15-3241-2015, https://www.atmos-chem-phys.net/15/3241/2015/, 2015.

di Sarra, A., Di Iorio, T., Cacciani, M., Fiocco, G., and Fuà, D.: Saharan dust profiles measured by lidar at Lampedusa, Journal of Geophysical Research: Atmospheres, 106, 10 335–10 347, doi:10.1029/2000JD900734, http://dx.doi.org/10.1029/2000JD900734, 2001.

Dubovik, O., Sinyuk, A., Lapyonok, T., Holben, B. N., Mishchenko, M., Yang, P., Eck, T. F., Volten, H., Muñoz, O., Veihelmann, B., van der Zande, W. J., Leon, J.-F., Sorokin, M., and Slutsker, I.: Application of spheroid models to account for aerosol particle nonsphericity in remote sensing of desert dust, Journal of Geophysical Research: Atmospheres, 111, n/a–n/a, doi:10.1029/2005JD006619, d11208, 2006.

Engelmann, R., Kanitz, T., Baars, H., Heese, B., Althausen, D., Skupin, A., Wandinger, U., Komppula, M., Stachlewska, I. S., Amiridis, V., Marinou, E., Mattis, I., Linné, H., and Ansmann, A.: The automated multiwavelength Raman polarization and water-vapor lidar PollyXT: the neXT generation, Atmospheric Measurement Techniques, 9, 1767–1784, doi:10.5194/amt-9-1767-2016, 2016.

Flamant, C., Trouillet, V., Chazette, P., and Pelon, J.: Wind speed dependence of atmospheric boundary layer optical properties and ocean surface reflectance as observed by airborne backscatter lidar, Journal of Geophysical Research: Oceans, 103, 25 137–25 158, doi:10.1029/98JC02284, http://dx.doi.org/10.1029/98JC02284, 1998.

Franke, K., Ansmann, A., Müller, D., Althausen, D., Venkataraman, C., Reddy, M. S., Wagner, F., and Scheele, R.: Optical properties of the Indo-Asian haze layer over the tropical Indian Ocean, Journal of Geophysical Research: Atmospheres, 108, n/a–n/a, doi:10.1029/2002JD002473, http://dx.doi.org/10.1029/2002JD002473, 4059, 2003.

Freudenthaler, V.: The telecover test: A quality assurance tool for the optical part of a lidar system, in: 24th International Laser Radar Conference, Boulder, CO, 2008.

Freudenthaler, V.: About the effects of polarising optics on lidar signals and the $\Delta 90$ calibration, Atmospheric Measurement Techniques, 9, 4181–4255, doi:10.5194/amt-9-4181-2016, 2016.

Freudenthaler, V., Esselborn, M., Wiegner, M., Heese, B., Tesche, M., Ansmann, A., Müller, D., Althausen, D., Wirth, M., Fix, A., Ehret, G., Knippertz, P., Toledano, C., Gasteiger, J., Garhammer, M., and Seefeldner, M.: Depolarization ratio profiling at several wavelengths in pure Saharan dust during SAMUM 2006, Tellus B, 61, 165–179, doi:10.1111/j.1600-0889.2008.00396.x, 2009.

Freudenthaler, V., Seefeldner, M., Groß, S., and Wandinger, U.: Accuracy of Linear Depolarisation Ratios in Clean Air Ranges Measured with POLIS-6 at 355 and 532 NM, EPJ Web of Conferences, 119, 25 013, doi:10.1051/epjconf/201611925013, 2016.

Garimella, S., Huang, Y.-W., Seewald, J. S., and Cziczo, D. J.: Cloud condensation nucleus activity comparison of dry- and wet-generated mineral dust aerosol: the significance of soluble material, Atmospheric Chemistry and Physics, 14, 6003–6019, doi:10.5194/acp-14-6003-2014, http://www.atmos-chem-phys.net/14/6003/2014/, 2014.

Gasteiger, J. and Freudenthaler, V.: Benefit of depolarization ratio at λ = 1064 nm for the retrieval of the aerosol microphysics from lidar measurements, Atmospheric Measurement Techniques, 7, 3773–3781, doi:10.5194/amt-7-3773-2014, 2014.

Gasteiger, J., Wiegner, M., Groß, S., Freudenthaler, V., Toledano, C., Tesche, M., and Kandler, K.: Modelling lidar-relevant optical properties of complex mineral dust aerosols, Tellus B, 63, 725–741, doi:10.1111/j.1600-0889.2011.00559.x, 2011.

Gasteiger, J., Groß, S., Sauer, D., Haarig, M., Ansmann, A., and Weinzierl, B.: Particle settling and vertical mixing in the Saharan Air Layer as seen from an integrated model, lidar, and in situ perspective, Atmospheric Chemistry and Physics, 17, 297–311, doi:10.5194/acp-17-297-2017, 2017.

Gimmestad, G. G.: Reexamination of depolarization in lidar measurements, Appl. Opt., 47, 3795–3802, doi:10.1364/AO.47.003795, 2008.

Gobbi, G. P.: Polarization lidar returns from aerosols and thin clouds: a framework for the analysis, Appl. Opt., 37, 5505–5508, doi:10.1364/AO.37.005505, http://ao.osa.org/abstract.cfm?URI=ao-37-24-5505, 1998.

Gobbi, G. P., Barnaba, F., Giorgi, R., and Santacasa, A.: Altitude-resolved properties of a Saharan dust event over the Mediterranean, Atmospheric Environment, 34, 5119 – 5127, doi:http://dx.doi.org/10.1016/S1352-2310(00)00194-1, http://www.sciencedirect.com/science/article/pii/S1352231000001941, sixth Scientific Conference of the International Global Atmospheric, 2000.

Groß, S., Gasteiger, J., Freudenthaler, V., Wiegner, M., Geiß, A., Schladitz, A., Toledano, C., Kandler, K., Tesche, M., Ansmann, A., and Wiedensohler, A.: Characterization of the planetary boundary layer during SAMUM-2 by means of lidar measurements, Tellus B, 63, 695–705, doi:10.1111/j.1600-0889.2011.00557.x, 2011a.

Groß, S., Tesche, M., Freudenthaler, V., Toledano, C., Wiegner, M., Ansmann, A., Althausen, D., and Seefeldner, M.: Characterization of Saharan dust, marine aerosols and mixtures of biomass-burning aerosols and dust by means of multi-wavelength depolarization and Raman lidar measurements during SAMUM 2, Tellus B, 63, 706–724, doi:10.1111/j.1600-0889.2011.00556.x, 2011b.

Groß, S., Freudenthaler, V., Schepanski, K., Toledano, C., Schäfler, A., Ansmann, A., and Weinzierl, B.: Optical properties of long-range transported Saharan dust over Barbados as measured by dual-wavelength depolarization Raman lidar measurements, Atmospheric Chemistry and Physics, 15, 11 067–11 080, doi:10.5194/acp-15-11067-2015, 2015.

Groß, S., Gasteiger, J., Freudenthaler, V., Müller, T., Sauer, D., Toledano, C., and Ansmann, A.: Saharan dust contribution to the Caribbean summertime boundary layer – a lidar study during SALTRACE, Atmospheric Chemistry and Physics, 16, 11 535–11 546, doi:10.5194/acp-16-11535-2016, http://www.atmos-chem-phys.net/16/11535/2016/, 2016.

Haarig, M., Althausen, D., Ansmann, A., Klepel, A., Baars, H., Engelmann, R., Groß, S., and Freudenthaler, V.: Measurement of the Linear Depolarization Ratio of Aged Dust at Three Wavelengths (355, 532 and 1064 nm) Simultaneously over Barbados, EPJ Web of Conferences, 119, 18 009, doi:10.1051/epjconf/201611918009, 2016a.

Haarig, M., Engelmann, R., Ansmann, A., Veselovskii, I., Whiteman, D. N., and Althausen, D.: 1064 nm rotational Raman lidar for particle extinction and lidar-ratio profiling: cirrus case study, Atmospheric Measurement Techniques, 9, 4269–4278, doi:10.5194/amt-9-4269-2016, 2016b.

Haarig, M., Ansmann, A., Gasteiger, J., Kandler, K., Althausen, D., Baars, H., and Farrell, D. A.: Dry versus wet marine particle optical properties: RH dependence of depolarization ratio, backscatter and extinction from multiwavelength lidar measurements during SALTRACE, Atmospheric Chemistry and Physics Discussions, 2017, 1–32, doi:10.5194/acp-2017-545, https://www.atmos-chem-phys-discuss.net/acp-2017-545/, 2017.

Haywood, J. M., Pelon, J., Formenti, P., Bharmal, N., Brooks, M., Capes, G., Chazette, P., Chou, C., Christopher, S., Coe, H., Cuesta, J., Derimian, Y., Desboeufs, K., Greed, G., Harrison, M., Heese, B., Highwood, E. J., Johnson, B., Mallet, M., Marticorena, B., Marsham, J., Milton, S., Myhre, G., Osborne, S. R., Parker, D. J., Rajot, J.-L., Schulz, M., Slingo, A., Tanré, D., and Tulet, P.: Overview of the Dust and Biomass-burning Experiment and African Monsoon Multidisciplinary Analysis Special Observing Period-0, Journal of Geophysical Research: Atmospheres, 113, n/a–n/a, doi:10.1029/2008JD010077, http://dx.doi.org/10.1029/2008JD010077, d00C17, 2008.

Heinold, B., Tegen, I., Schepanski, K., Tesche, M., Esselborn, M., Freudenthaler, V., Groß, S., Kandler, K., Knippertz, P., Müeller, D., Schladitz, A., Toledano, C., Weinzierl, B., Ansmann, A., Althausen, D., Müller, T., Petzold, A., and Wiedensohler, A.: Regional modelling of Saharan dust and biomass-burning smoke, Tellus B, 63, 781–799, doi:10.1111/j.1600-0889.2011.00570.x, 2011.

Heintzenberg, J.: The SAMUM-1 experiment over Southern Morocco: overview and introduction, Tellus B, 61, 2–11, doi:10.1111/j.1600-0889.2008.00403.x, 2009.

Hofer, J., Althausen, D., Abdullaev, S. F., Makhmudov, A. N., Nazarov, B. I., Schettler, G., Engelmann, R., Baars, H., Fomba, K. W., Müller, K., Heinold, B., Kandler, K., and Ansmann, A.: Long-term profiling of mineral dust and pollution aerosol with multiwavelength polarization/Raman lidar at the Central Asian site of Dushanbe, Tajikistan: Case studies, Atmospheric Chemistry and Physics Discussions, 2017, 1–34, doi:10.5194/acp-2017-559, https://www.atmos-chem-phys-discuss.net/acp-2017-559/, 2017.

Holben, B., Eck, T., Slutsker, I., Tanré, D., Buis, J., Setzer, A., Vermote, E., Reagan, J., Kaufman, Y., Nakajima, T., Lavenu, F., Jankowiak, I., and Smirnov, A.: AERONET—A Federated Instrument Network and Data Archive for Aerosol Characterization, Remote Sensing of Environment, 66, 1 – 16, doi:http://dx.doi.org/10.1016/S0034-4257(98)00031-5, http://www.sciencedirect.com/science/article/pii/S0034425798000315, 1998.

Huebert, B. J., Bates, T., Russell, P. B., Shi, G., Kim, Y. J., Kawamura, K., Carmichael, G., and Nakajima, T.: An overview of ACE-Asia: Strategies for quantifying the relationships between Asian aerosols and their climatic impacts, Journal of Geophysical Research: Atmospheres, 108, n/a–n/a, doi:10.1029/2003JD003550, http://dx.doi.org/10.1029/2003JD003550, 8633, 2003.

Huneeus, N., Schulz, M., Balkanski, Y., Griesfeller, J., Prospero, J., Kinne, S., Bauer, S., Boucher, O., Chin, M., Dentener, F., Diehl, T., Easter, R., Fillmore, D., Ghan, S., Ginoux, P., Grini, A., Horowitz, L., Koch, D., Krol, M. C., Landing, W., Liu, X., Mahowald, N., Miller, R., Morcrette, J.-J., Myhre, G., Penner, J., Perlwitz, J., Stier, P., Takemura, T., and Zender, C. S.: Global dust model intercomparison in AeroCom phase I, Atmospheric Chemistry and Physics, 11, 7781–7816, doi:10.5194/acp-11-7781-2011, https://www.atmos-chem-phys.net/11/7781/2011/, 2011.

HYSPLIT: HYbrid Single-Particle Lagrangian Integrated Trajectory model, backward trajectory calculation tool, http://ready.arl.noaa.gov/HYSPLIT.php, 2016.

Iwasaka, Y., Yamato, M., Imasu, R., and Ono, A.: Transport of Asian dust (KOSA) particles; importance of weak KOSA events on the geochemical cycle of soil particles, Tellus B, 40B, 494–503, doi:10.1111/j.1600-0889.1988.tb00119.x, http://dx.doi.org/10.1111/j.1600-0889.1988.tb00119.x, 1988.

Jähn, M., Muñoz-Esparza, D., Chouza, F., Reitebuch, O., Knoth, O., Haarig, M., and Ansmann, A.: Investigations of boundary layer structure, cloud characteristics and vertical mixing of aerosols at Barbados with large eddy simulations, Atmospheric Chemistry and Physics, 16, 651–674, doi:10.5194/acp-16-651-2016, 2016.

Järvinen, E., Kemppinen, O., Nousiainen, T., Kociok, T., Möhler, O., Leisner, T., and Schnaiter, M.: Laboratory investigations of mineral dust near-backscattering depolarization ratios, Journal of Quantitative Spectroscopy and Radiative Transfer, 178, 192 – 208, doi:http://dx.doi.org/10.1016/j.jqsrt.2016.02.003, http://www.sciencedirect.com/science/article/pii/S0022407315301722, 2016.

Johnson, B. T. and Osborne, S. R.: Physical and optical properties of mineral dust aerosol measured by aircraft during the GERBILS campaign, Quarterly Journal of the Royal Meteorological Society, 137, 1117–1130, doi:10.1002/qj.777, http://dx.doi.org/10.1002/qj.777, 2011.

Jung, E., Albrecht, B., Prospero, J. M., Jonsson, H. H., and Kreidenweis, S. M.: Vertical structure of aerosols, temperature, and moisture associated with an intense African dust event observed over the eastern Caribbean, Journal of Geophysical Research: Atmospheres, 118, 4623–4643, doi:10.1002/jgrd.50352, http://dx.doi.org/10.1002/jgrd.50352, 2013.

Kanitz, T., Ansmann, A., Engelmann, R., and Althausen, D.: North-south cross sections of the vertical aerosol distribution over the Atlantic Ocean from multiwavelength Raman/polarization lidar during Polarstern cruises, Journal of Geophysical Research: Atmospheres, 118, 2643–2655, doi:10.1002/jgrd.50273, 2013.

Kanitz, T., Engelmann, R., Heinold, B., Baars, H., Skupin, A., and Ansmann, A.: Tracking the Saharan Air Layer with shipborne lidar across the tropical Atlantic, Geophysical Research Letters, 41, 1044–1050, doi:10.1002/2013GL058780, 2014.

Karyampudi, V. M., Palm, S. P., Reagen, J. A., Fang, H., Grant, W. B., Hoff, R. M., Moulin, C., Pierce, H. F., Torres, O., Browell, E. V., and Melfi, S. H.: Validation of the Saharan Dust Plume Conceptual Model Using Lidar, Meteosat, and ECMWF Data, Bulletin of the American Meteorological Society, 80, 1045–1075, doi:10.1175/1520-0477(1999)080<1045:VOTSDP>2.0.CO;2, https://doi.org/10.1175/1520-0477(1999)080<1045:VOTSDP>2.0.CO;2, 1999.

Kemppinen, O., Nousiainen, T., and Lindqvist, H.: The impact of surface roughness on scattering by realistically shaped wavelength-scale dust particles, Journal of Quantitative Spectroscopy and Radiative Transfer, 150, 55 – 67, doi:http://dx.doi.org/10.1016/j.jqsrt.2014.05.024, topical issue on optical particle characterization and remote sensing of the atmosphere: Part I, 2015a.

Kemppinen, O., Nousiainen, T., Merikallio, S., and Räisänen, P.: Retrieving microphysical properties of dust-like particles using ellipsoids: the case of refractive index, Atmospheric Chemistry and Physics, 15, 11 117–11 132, doi:10.5194/acp-15-11117-2015, 2015b.

Kobayashi, A., Hayashida, S., Okada, K., and Iwasaka, Y.: Measurements of the Polarization Properties of Kosa (Asian Dust-storm) Particles by a Laser Radar in Spring 1983, Journal of the Meteorological Society of Japan. Ser. II, 63, 144–149, doi:10.2151/jmsj1965.63.1_144, 1985.

Kristensen, T. B., Müller, T., Kandler, K., Benker, N., Hartmann, M., Prospero, J. M., Wiedensohler, A., and Stratmann, F.: Properties of cloud condensation nuclei (CCN) in the trade wind marine boundary layer of the western North Atlantic, Atmospheric Chemistry and Physics, 16, 2675–2688, doi:10.5194/acp-16-2675-2016, http://www.atmos-chem-phys.net/16/2675/2016/, 2016.

Lindqvist, H., Jokinen, O., Kandler, K., Scheuvens, D., and Nousiainen, T.: Single scattering by realistic, inhomogeneous mineral dust particles with stereogrammetric shapes, Atmospheric Chemistry and Physics, 14, 143–157, doi:10.5194/acp-14-143-2014, http://www.atmos-chem-phys.net/14/143/2014/, 2014.

Liu, L., Mishchenko, M. I., Hovenier, J. W., Volten, H., and Muñoz, O.: Scattering matrix of quartz aerosols: comparison and synthesis of laboratory and Lorenz–Mie results, Journal of Quantitative Spectroscopy and Radiative Transfer, 79, 911 – 920, doi:http://dx.doi.org/10.1016/S0022-4073(02)00328-X, http://www.sciencedirect.com/science/article/pii/S002240730200328X, electromagnetic and Light Scattering by Non-Spherical Particles, 2003.

Lopatin, A., Dubovik, O., Chaikovsky, A., Goloub, P., Lapyonok, T., Tanré, D., and Litvinov, P.: Enhancement of aerosol characterization using synergy of lidar and sun-photometer coincident observations: the GARRLiC algorithm, Atmospheric Measurement Techniques, 6, 2065–2088, doi:10.5194/amt-6-2065-2013, 2013.

Mamouri, R. E. and Ansmann, A.: Fine and coarse dust separation with polarization lidar, Atmospheric Measurement Techniques, 7, 3717–3735, doi:10.5194/amt-7-3717-2014, 2014.

Mamouri, R.-E. and Ansmann, A.: Potential of polarization/Raman lidar to separate fine dust, coarse dust, maritime, and anthropogenic aerosol profiles, Atmospheric Measurement Techniques Discussions, 2017, 1–41, doi:10.5194/amt-2017-131, https://www.atmos-meas-tech-discuss.net/amt-2017-131/, 2017.

Marinou, E., Amiridis, V., Binietoglou, I., Tsikerdekis, A., Solomos, S., Proestakis, E., Konsta, D., Papagiannopoulos, N., Tsekeri, A., Vlastou, G., Zanis, P., Balis, D., Wandinger, U., and Ansmann, A.: Three-dimensional evolution of Saharan dust transport to-

wards Europe based on a 9-year EARLINET-optimized CALIPSO dataset, Atmospheric Chemistry and Physics, 17, 5893–5919, doi:10.5194/acp-17-5893-2017, http://www.atmos-chem-phys.net/17/5893/2017/, 2017.

Mattis, I., Ansmann, A., Müller, D., Wandinger, U., and Althausen, D.: Dual-wavelength Raman lidar observations of the extinction-to-backscatter ratio of Saharan dust, Geophysical Research Letters, 29, 20–1–20–4, doi:10.1029/2002GL014721, http://dx.doi.org/10.1029/2002GL014721, 2002.

Mattis, I., Tesche, M., Grein, M., Freudenthaler, V., and Müller, D.: Systematic error of lidar profiles caused by a polarization-dependent receiver transmission: quantification and error correction scheme, Appl. Opt., 48, 2742–2751, doi:10.1364/AO.48.002742, 2009.

McConnell, C. L., Highwood, E. J., Coe, H., Formenti, P., Anderson, B., Osborne, S., Nava, S., Desboeufs, K., Chen, G., and Harrison, M. A. J.: Seasonal variations of the physical and optical characteristics of Saharan dust: Results from the Dust Outflow and Deposition to the Ocean (DODO) experiment, Journal of Geophysical Research: Atmospheres, 113, n/a–n/a, doi:10.1029/2007JD009606, http://dx.doi.org/10.1029/2007JD009606, d14S05, 2008.

McNeil, W. R. and Carsweil, A. l.: Lidar polarization studies of the troposphere, Appl. Opt., 14, 2158–2168, doi:10.1364/AO.14.002158, http://ao.osa.org/abstract.cfm?URI=ao-14-9-2158, 1975.

Miffre, A., Mehri, T., Francis, M., and Rairoux, P.: UV–VIS depolarization from Arizona Test Dust particles at exact backscattering angle, Journal of Quantitative Spectroscopy and Radiative Transfer, 169, 79 – 90, doi:http://dx.doi.org/10.1016/j.jqsrt.2015.09.016, http://www.sciencedirect.com/science/article/pii/S0022407315300285, 2016.

Müller, D., Ansmann, A., Freudenthaler, V., Kandler, K., Toledano, C., Hiebsch, A., Gasteiger, J., Esselborn, M., Tesche, M., Heese, B., Althausen, D., Weinzierl, B., Petzold, A., and von Hoyningen-Huene, W.: Mineral dust observed with AERONET Sun photometer, Raman lidar, and in situ instruments during SAMUM 2006: Shape-dependent particle properties, Journal of Geophysical Research: Atmospheres, 115, n/a–n/a, doi:10.1029/2009JD012523, d11207, 2010a.

Müller, D., Weinzierl, B., Petzold, A., Kandler, K., Ansmann, A., Müller, T., Tesche, M., Freudenthaler, V., Esselborn, M., Heese, B., Althausen, D., Schladitz, A., Otto, S., and Knippertz, P.: Mineral dust observed with AERONET Sun photometer, Raman lidar, and in situ instruments during SAMUM 2006: Shape-independent particle properties, Journal of Geophysical Research: Atmospheres, 115, n/a–n/a, doi:10.1029/2009JD012520, d07202, 2010b.

Müller, D., Lee, K.-H., Gasteiger, J., Tesche, M., Weinzierl, B., Kandler, K., Müller, T., Toledano, C., Otto, S., Althausen, D., and Ansmann, A.: Comparison of optical and microphysical properties of pure Saharan mineral dust observed with AERONET Sun photometer, Raman lidar, and in situ instruments during SAMUM 2006, Journal of Geophysical Research: Atmospheres, 117, n/a–n/a, doi:10.1029/2011JD016825, d07211, 2012.

Müller, D., Veselovskii, I., Kolgotin, A., Tesche, M., Ansmann, A., and Dubovik, O.: Vertical profiles of pure dust and mixed smoke-dust plumes inferred from inversion of multiwavelength Raman/polarization lidar data and comparison to AERONET retrievals and in situ observations, Appl. Opt., 52, 3178–3202, doi:10.1364/AO.52.003178, 2013.

Murayama, T., Sugimoto, N., Uno, I., Kinoshita, K., Aoki, K., Hagiwara, N., Liu, Z., Matsui, I., Sakai, T., Shibata, T., Arao, K., Sohn, B.-J., Won, J.-G., Yoon, S.-C., Li, T., Zhou, J., Hu, H., Abo, M., Iokibe, K., Koga, R., and Iwasaka, Y.: Ground-based network observation of Asian dust events of April 1998 in east Asia, Journal of Geophysical Research: Atmospheres, 106, 18 345–18 359, doi:10.1029/2000JD900554, http://dx.doi.org/10.1029/2000JD900554, 2001.

Omar, A. H., Winker, D. M., Vaughan, M. A., Hu, Y., Trepte, C. R., Ferrare, R. A., Lee, K.-P., Hostetler, C. A., Kittaka, C., Rogers, R. R., Kuehn, R. E., and Liu, Z.: The CALIPSO Automated Aerosol Classification and Lidar Ratio Selection Algorithm, Journal of Atmospheric and Oceanic Technology, 26, 1994–2014, doi:10.1175/2009JTECHA1231.1, https://doi.org/10.1175/2009JTECHA1231.1, 2009.

Papayannis, A., Balis, D., Amiridis, V., Chourdakis, G., Tsaknakis, G., Zerefos, C., Castanho, A. D. A., Nickovic, S., Kazadzis, S., and Grabowski, J.: Measurements of Saharan dust aerosols over the Eastern Mediterranean using elastic backscatter-Raman lidar, spectrophotometric and satellite observations in the frame of the EARLINET project, Atmospheric Chemistry and Physics, 5, 2065–2079, doi:10.5194/acp-5-2065-2005, https://www.atmos-chem-phys.net/5/2065/2005/, 2005.

5   Preißler, J., Wagner, F., Pereira, S. N., and Guerrero-Rascado, J. L.: Multi-instrumental observation of an exceptionally strong Saharan dust outbreak over Portugal, Journal of Geophysical Research: Atmospheres, 116, n/a–n/a, doi:10.1029/2011JD016527, http://dx.doi.org/10.1029/2011JD016527, d24204, 2011.

Reid, J. S., Kinney, J. E., Westphal, D. L., Holben, B. N., Welton, E. J., Tsay, S.-C., Eleuterio, D. P., Campbell, J. R., Christopher, S. A., Colarco, P. R., Jonsson, H. H., Livingston, J. M., Maring, H. B., Meier, M. L., Pilewskie, P., Prospero, J. M., Reid, E. A., Remer, L. A.,

10   Russell, P. B., Savoie, D. L., Smirnov, A., and Tanré, D.: Analysis of measurements of Saharan dust by airborne and ground-based remote sensing methods during the Puerto Rico Dust Experiment (PRIDE), Journal of Geophysical Research: Atmospheres, 108, n/a–n/a, doi:10.1029/2002JD002493, http://dx.doi.org/10.1029/2002JD002493, 8586, 2003.

Rittmeister, F., Ansmann, A., Engelmann, R., Skupin, A., Baars, H., Kanitz, T., and Kinne, S.: Profiling of Saharan dust from the Caribbean to West Africa, Part 1: Layering structure and optical properties from shipborne polarization/ Ramn lidar obersverations, Atmospheric

15   Chemistry and Physics Discussions, 2017, 1–24, doi:10.5194/acp-2017-130, http://www.atmos-chem-phys-discuss.net/acp-2017-130/, revised version, 2017.

Ryder, C. L., Highwood, E. J., Rosenberg, P. D., Trembath, J., Brooke, J. K., Bart, M., Dean, A., Crosier, J., Dorsey, J., Brindley, H., Banks, J., Marsham, J. H., McQuaid, J. B., Sodemann, H., and Washington, R.: Optical properties of Saharan dust aerosol and contribution from the coarse mode as measured during the Fennec 2011 aircraft campaign, Atmospheric Chemistry and Physics, 13, 303–325,

20   doi:10.5194/acp-13-303-2013, https://www.atmos-chem-phys.net/13/303/2013/, 2013.

Sakai, T., Nagai, T., Zaizen, Y., and Mano, Y.: Backscattering linear depolarization ratio measurements of mineral, sea-salt, and ammonium sulfate particles simulated in a laboratory chamber, Appl. Opt., 49, 4441–4449, doi:10.1364/AO.49.004441, 2010.

Shimizu, A., Sugimoto, N., Matsui, I., Arao, K., Uno, I., Murayama, T., Kagawa, N., Aoki, K., Uchiyama, A., and Yamazaki, A.: Continuous observations of Asian dust and other aerosols by polarization lidars in China and Japan during ACE-Asia, Journal of Geophysical Research:

25   Atmospheres, 109, n/a–n/a, doi:10.1029/2002JD003253, http://dx.doi.org/10.1029/2002JD003253, d19S17, 2004.

Solomos, S., Ansmann, A., Mamouri, R.-E., Binietoglou, I., Patlakas, P., Marinou, E., and Amiridis, V.: Remote sensing and modelling analysis of the extreme dust storm hitting the Middle East and eastern Mediterranean in September 2015, Atmospheric Chemistry and Physics, 17, 4063–4079, doi:10.5194/acp-17-4063-2017, https://www.atmos-chem-phys.net/17/4063/2017/, 2017.

Stein, A. F., Draxler, R. R., Rolph, G. D., Stunder, B. J. B., Cohen, M. D., and Ngan, F.: NOAA's HYSPLIT Atmospheric Transport and

30   Dispersion Modeling System, Bulletin of the American Meteorological Society, 96, 2059–2077, doi:10.1175/BAMS-D-14-00110.1, 2015.

Stevens, B., Farrell, D., Hirsch, L., Jansen, F., Nuijens, L., Serikov, I., Brügmann, B., Forde, M., Linne, H., Lonitz, K., and Prospero, J. M.: The Barbados Cloud Observatory: Anchoring Investigations of Clouds and Circulation on the Edge of the ITCZ, Bulletin of the American Meteorological Society, 97, 787–801, doi:10.1175/BAMS-D-14-00247.1, https://doi.org/10.1175/BAMS-D-14-00247.1, 2016.

Sugimoto, N. and Lee, C. H.: Characteristics of dust aerosols inferred from lidar depolarization measurements at two wavelengths, Appl.

35   Opt., 45, 7468–7474, doi:10.1364/AO.45.007468, 2006.

Tanré, D., Haywood, J., Pelon, J., Léon, J. F., Chatenet, B., Formenti, P., Francis, P., Goloub, P., Highwood, E. J., and Myhre, G.: Measurement and modeling of the Saharan dust radiative impact: Overview of the Saharan Dust Experiment (SHADE), Journal of Geophysical Research: Atmospheres, 108, n/a–n/a, doi:10.1029/2002JD003273, http://dx.doi.org/10.1029/2002JD003273, 8574, 2003.

Tesche, M., Ansmann, A., Müller, D., Althausen, D., Mattis, I., Heese, B., Freudenthaler, V., Wiegner, M., Esselborn, M., Pisani, G., and Knippertz, P.: Vertical profiling of Saharan dust with Raman lidars and airborne HSRL in southern Morocco during SAMUM, Tellus B, 61, 144–164, doi:10.1111/j.1600-0889.2008.00390.x, 2009.

Tesche, M., Gross, S., Ansmann, A., Müller, D. D., Althausen, D., Freudenthaler, V., and Esselborn, M.: Profiling of Saharan dust and biomass-burning smoke with multiwavelength polarization Raman lidar at Cape Verde, Tellus B, 63, 649–676, doi:10.1111/j.1600-0889.2011.00548.x, 2011a.

Tesche, M., Müller, D., Gross, S., Ansmann, A., Althausen, D., Freudenthaler, V., Weinzierl, B., Veira, A., and Petzold, A.: Optical and microphysical properties of smoke over Cape Verde inferred from multiwavelength lidar measurements, Tellus B, 63, 677–694, doi:10.1111/j.1600-0889.2011.00549.x, 2011b.

Tesche, M., Wandinger, U., Ansmann, A., Althausen, D., Müller, D., and Omar, A. H.: Ground-based validation of CALIPSO observations of dust and smoke in the Cape Verde region, Journal of Geophysical Research: Atmospheres, 118, 2889–2902, doi:10.1002/jgrd.50248, 2013.

Toledano, C., Wiegner, M., Garhammer, M., Seefeldner, M., Gasteiger, J., Müeller, D., and Koepke, P.: Spectral aerosol optical depth characterization of desert dust during SAMUM 2006, Tellus B, 61, 216–228, doi:10.1111/j.1600-0889.2008.00382.x, 2009.

Toledano, C., Wiegner, M., Groß, S., Freudenthaler, V., Gasteiger, J., Müeller, D., Müeller, T., Schladitz, A., Weinzierl, B., Torres, B., and O'Neill, N. T.: Optical properties of aerosol mixtures derived from sun-sky radiometry during SAMUM-2, Tellus B, 63, 635–648, doi:10.1111/j.1600-0889.2011.00573.x, 2011.

Veselovskii, I., Dubovik, O., Kolgotin, A., Lapyonok, T., Di Girolamo, P., Summa, D., Whiteman, D. N., Mishchenko, M., and Tanré, D.: Application of randomly oriented spheroids for retrieval of dust particle parameters from multiwavelength lidar measurements, Journal of Geophysical Research: Atmospheres, 115, n/a–n/a, doi:10.1029/2010JD014139, d21203, 2010.

Veselovskii, I., Goloub, P., Podvin, T., Bovchaliuk, V., Derimian, Y., Augustin, P., Fourmentin, M., Tanre, D., Korenskiy, M., Whiteman, D. N., Diallo, A., Ndiaye, T., Kolgotin, A., and Dubovik, O.: Retrieval of optical and physical properties of African dust from multiwavelength Raman lidar measurements during the SHADOW campaign in Senegal, Atmospheric Chemistry and Physics, 16, 7013–7028, doi:10.5194/acp-16-7013-2016, 2016.

Volten, H., Muñoz, O., Rol, E., de Haan, J. F., Vassen, W., Hovenier, J. W., Muinonen, K., and Nousiainen, T.: Scattering matrices of mineral aerosol particles at 441.6 nm and 632.8 nm, Journal of Geophysical Research: Atmospheres, 106, 17 375–17 401, doi:10.1029/2001JD900068, http://dx.doi.org/10.1029/2001JD900068, 2001.

Wagner, J., Ansmann, A., Wandinger, U., Seifert, P., Schwarz, A., Tesche, M., Chaikovsky, A., and Dubovik, O.: Evaluation of the Lidar/Radiometer Inversion Code (LIRIC) to determine microphysical properties of volcanic and desert dust, Atmospheric Measurement Techniques, 6, 1707–1724, doi:10.5194/amt-6-1707-2013, 2013.

Wandinger, U. and Ansmann, A.: Experimental Determination of the Lidar Overlap Profile with Raman Lidar, Appl. Opt., 41, 511–514, doi:10.1364/AO.41.000511, 2002.

Wandinger, U., Müller, D., Böckmann, C., Althausen, D., Matthias, V., Bösenberg, J., Weiß, V., Fiebig, M., Wendisch, M., Stohl, A., and Ansmann, A.: Optical and microphysical characterization of biomass- burning and industrial-pollution aerosols from- multiwavelength lidar and aircraft measurements, Journal of Geophysical Research: Atmospheres, 107, LAC 7–1–LAC 7–20, doi:10.1029/2000JD000202, http://dx.doi.org/10.1029/2000JD000202, 8125, 2002.

Weinzierl, B., Ansmann, A., Prospero, J. M., Althausen, D., Benker, N., Chouza, F., Dollner, M., Farrell, D., Fomba, W. K., Freudenthaler, V., Gasteiger, J., Groß, S., Haarig, M., Heinold, B., Kandler, K., Kristensen, T. B., Mayol-Bracero, O. L., Müller, T., Reitebuch, O., Sauer, D.,

30

Schäfler, A., Schepanski, K., Spanu, A., Tegen, I., Toledano, C., and Walser, A.: The Saharan Aerosol Long-range Transport and Aerosol-Cloud-Interaction Experiment (SALTRACE): overview and selected highlights, Bulletin of the American Meteorological Society, 0, null, doi:10.1175/BAMS-D-15-00142.1, 2017.

West, R. A., Doose, L. R., Eibl, A. M., Tomasko, M. G., and Mishchenko, M. I.: Laboratory measurements of mineral dust scattering phase function and linear polarization, Journal of Geophysical Research: Atmospheres, 102, 16 871–16 881, doi:10.1029/96JD02584, http://dx.doi.org/10.1029/96JD02584, 1997.

Wex, H., Dieckmann, K., Roberts, G. C., Conrath, T., Izaguirre, M. A., Hartmann, S., Herenz, P., Schäfer, M., Ditas, F., Schmeissner, T., Henning, S., Wehner, B., Siebert, H., and Stratmann, F.: Aerosol arriving on the Caribbean island of Barbados: physical properties and origin, Atmospheric Chemistry and Physics, 16, 14 107–14 130, doi:10.5194/acp-16-14107-2016, http://www.atmos-chem-phys.net/16/14107/2016/, 2016.

Wiegner, M., Gasteiger, J., Kandler, K., Weinzierl, B., Rasp, K., Esselborn, M., Freudenthaler, V., Heese, B., Toledano, C., Tesche, M., and Althausen, D.: Numerical simulations of optical properties of Saharan dust aerosols with emphasis on lidar applications, Tellus B, 61, 180–194, doi:10.1111/j.1600-0889.2008.00381.x, 2009.

Table 1. Main system parameters the BERTHA and POLIS lidar systems.

Property	BERTHA	POLIS
Emitted wavelengths (nm)	355, 532, 1064	355, 532
Pulse energy (mJ) [*]	120 + 800 + 1000	50 + 27
Repetition rate (Hz)	30	10
Telescope	Cassegrain	Dall-Kirkham
Eff. telescope diameter (m)	0.53	0.175
Receiver field of view (mrad)	0.8	2.5
Detected wavelenghts (nm)		
- elastic (total)	355, 532, 1064	
- co-polarized		355, 532
- cross-polarized	355, 532, 1064	355, 532
- inelastic (vib. Raman)	387, 407, 607	387, 607
- further	532_{HSRL}, 532_{RR},	
Range resolution (m)	7.5	3.75

HSRL - High Spectral Resolution Lidar; RR - Rotational Raman

[*] internal attenuation are not taken into account for BERTHA, but for POLIS

Table 2. SALTRACE mean particle linear depolarization ratio and corresponding standard deviation (SD), for all three wavelengths, observed within the Saharan dust layer with BERTHA in June and July 2013 and June and July 2014. Typical uncertainties in the retrieval of individual particle depolarization ratio values (systematic errors) are given for comparison. These uncertainties consider the volume depolarization retrieval uncertainties (see Appendix) and uncertainties in the backscatter coefficients required as input in addition.

Wavelength	Mean	SD	Syst. error
355 nm	**0.252**	**0.030**	**0.074**
532 nm	**0.280**	**0.020**	**0.019**
1064 nm	**0.225**	**0.022**	0.008

Table 3. BERTHA parameters (values) used in the volume depolarization ratio retrieval and uncertainties. Each wavelength is treated separately. **Rotational misalignment of the laser (α), of the emitting optics (β), the receiving optics (γ) and the cross polarized receiver channel (ν_R); diattenuation and retardation of the emitter optics(D_E, Δ_E) and the receiver optics (D_0, Δ_E); the diattenuation of the total and cross-polarized receiver channel (D_R,D_T); the degree of linear polarization of the beam expander (a_{BE}) and the polarization parameter of the 90°-mirror in the telescope (a_0).** Explanation for the parameters are given in the text. The configuration is given for SALTRACE-3 (summer 2014).

Property	355 nm		532 nm		1064 nm	
	Value	Uncertainty	Value	Uncertainty	Value	Uncertainty
α	0.9°	± 0.2°	1.1°	± 0.1°	0.9°	± 0.2°
D_E	0.049	± 0.034	0.046	± 0.028	0.047	± 0.037
Δ_E	0°	± 180°	0°	± 180°	0°	± 180°
β	0°	± 1°	0°	± 1°	0°	± 1°
a_{BE}	0.97	± 0.02	1.00	-0.01	1.00	- 0.01
D_0	0.07	± 0.02	**-0.057**	± 0.005	0.040	± 0.01
Δ_0	0°	± 180°	0°	± 180°	0°	± 180°
γ	0°	± 0.2°	0°	± 0.2°	0°	± 0.2°
a_0	**1.00**	**-0.01**	**0.958**	**± 0.005**	**1.00**	**-0.01**
D_T	0.07	± 0.01	**0.088**	± 0.01	0.080	± 0.01
D_R	-0.903	± 0.01	**-0.992**	± 0.01	-0.980	± 0.01
ν_R	0°	± 0.5°	0°	± 0.5°	0°	± 0.5°

Table 4. The results of the simulation of the lidar system for the volume linear depolarization ratio. The simulation has been performed for the theoretical Rayleigh background and a typical value for the dust layer for each wavelength. The maximum and minimum value for each simulation and its standard deviation is given.

| Wavelength	Rayleigh				Dust layer			
	input	min	max	std	input	min	max	std
355 nm	0.0080	**-0.0130**	0.0440	0.0995	0.080	**0.056**	**0.118**	**0.010**
532 nm	0.0053	**-0.0020**	0.0260	0.0049	0.200	**0.188**	**0.224**	**0.006**
1064 nm	0.0036	**-0.0050**	0.0250	0.0057	0.230	**0.214**	**0.257**	**0.007**
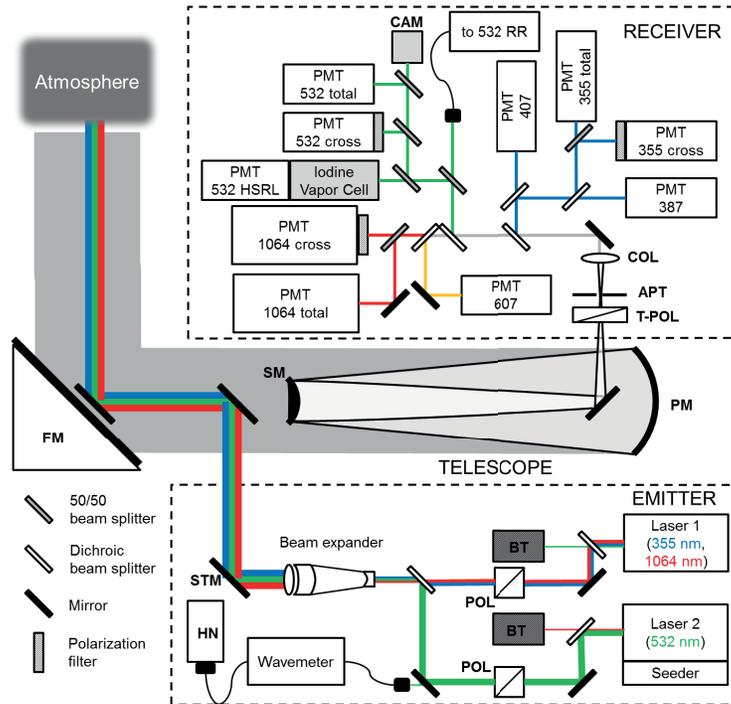
Figure 1. Sketch of BERTHA's emitter and receiver. All detection channels are photomultiplier tubes (PMT, operated in the photon counting mode), the number indicate the **central wavelength of transmission** in nanometer of the interference filter. Polarization filters perpendicular oriented to the emitted state of polarization are placed in front of the 'cross' channels, the 'total' channels measure the cross and the parallel part of the backscattered light, POL denotes polarizer to purify the laser polarization, BT beam trap, HN helium neon laser as reference for the wavemeter, STM steering mirror **with stepper motors** to adjust the overlap, CAM camera to **visualize** the overlap, FM flat mirror, **consisting of two mirrors, the small one for emitted pulses, the large one for backscattered light,** respectively, PM stands for main or primary mirror and SM for counter or secondary mirror of the Cassegrain telescope, TPOL means turnable polarization filter for Δ 90° calibration, APT motorized aperture, and COL collimator. Finally RR denotes rotational Raman channel, and HSRL High Spectral Resolution Lidar channel.
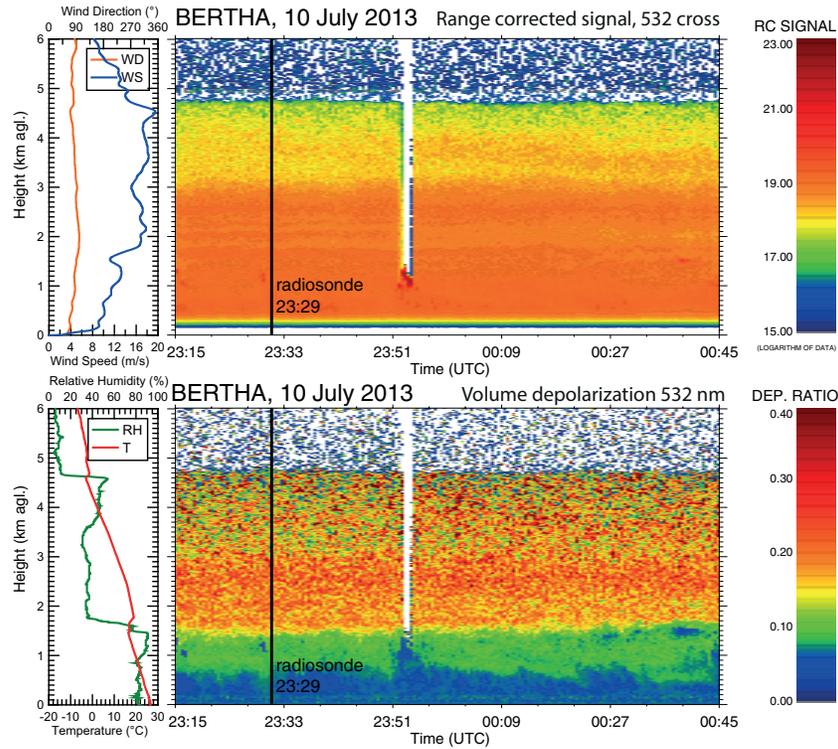
Figure 2. Saharan air layer (from 1.5–4.7 km height above ground level) above the marine boundary layer. The upper right panel shows the range-corrected cross-polarized 532 nm backscatter signal with temporal and vertical resolution of 30 s and 7.5 m, respectively. The lower right panel shows the 532 nm volume linear depolarization ratio. The lidar observation was performed on 10 July 2013, 19:15–20:45 local time. A radiosonde was launched at 19:29 local time (indicated by black vertical lines). The radiosonde profiles of wind speed (WS) and wind direction (WD) are shown in the upper left panel, the profiles of relative humidity (RH) and temperature (T) in the lower left panel.
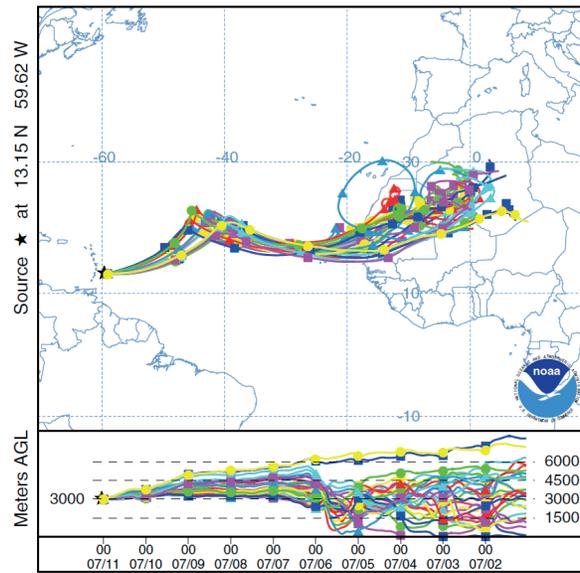
Figure 3. Ensemble of 10-day backward trajectories (Stein et al., 2015; HYSPLIT, 2016) for 11 July 2013, 0100 UTC, arriving at at 3000 m over Barbados.
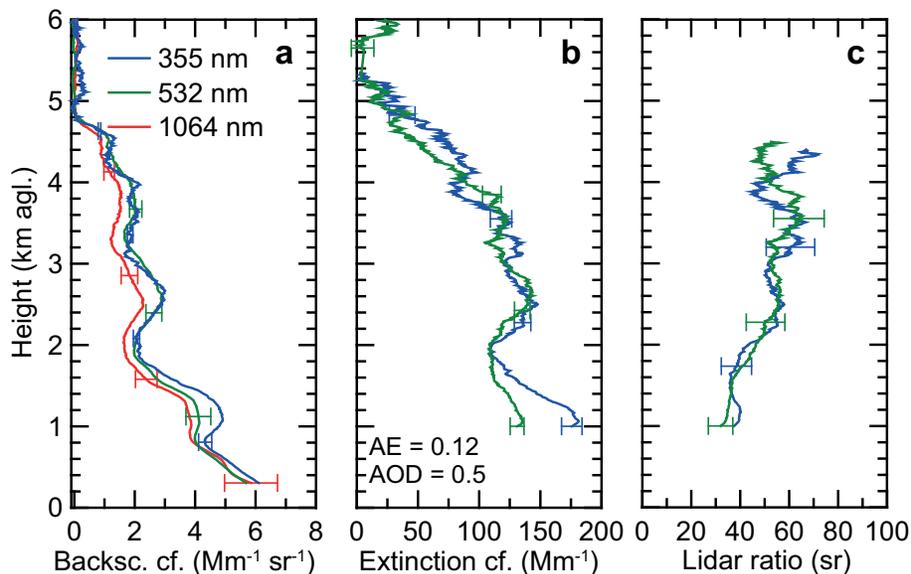
Figure 4. 45-minute mean profiles of (a) the particle backscatter coefficient at three wavelengths, (b) extinction coefficient at two wavelengths, and (c) extinction-to-backscatter ratio (lidar ratio) at two wavelengths, measured with BERTHA on 11 July 2013, 00:00–00:45 UTC. Error bars indicate the retrieval uncertainty (one standard deviation). The vertical signal smoothing window length is 200 m (backscatter coefficient) and 1000 m (extinction coefficient, lidar ratio). **The column values of the Ångström exponent (AE 440-870 nm) and the aerosol optical depth (AOD) from the closest AERONET observation are indicated.**
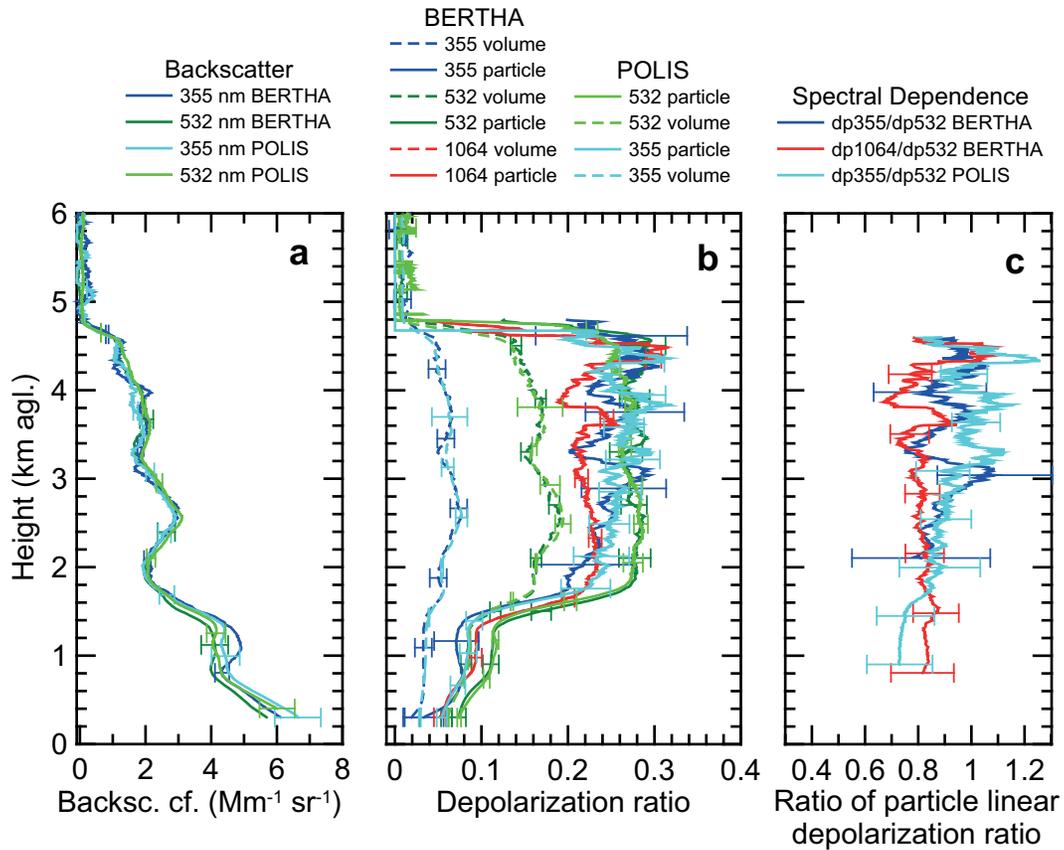
Figure 5. Comparison of POLIS and BERTHA depolarization-ratio observations. Shown are 45-minute mean profiles of (a) the particle backscatter coefficient at 355 (POLIS light blue, BERTHA dark blue) and 532 nm wavelength (POLIS light green, BERTHA dark green), (b) volume (dashed curves) and particle linear depolarization ratio (solid lines) at 355 nm (POLIS light blue, BERTHA dark blue), 532 nm (POLIS light green, BERTHA dark green), and 1064 nm (BERTHA, red line, equal volume and particle depolarization ratio profiles), (c) ratio of the 355 nm to 532 nm particle depolarization ratio (POLIS light blue, BERTHA dark blue) and 1064 nm to 532 nm particle depolarization ratio (BERTHA, red). POLIS and BERTHA observations were taken simultaneously on 11 July 2013, 00:00–00:45 UTC. Error bars indicate the retrieval uncertainty (one standard deviation). The vertical signal smoothing window length is 200 m (BERTHA, POLIS).
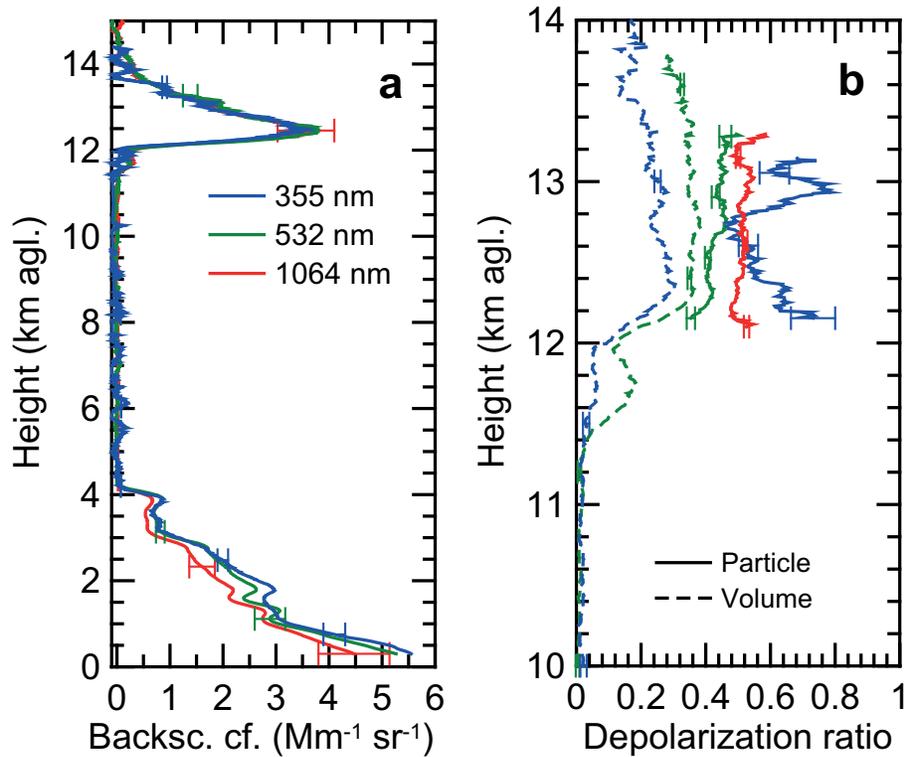
Figure 6. (a) Aerosol layers below 4 km height and cirrus layer from 12–14 km height in terms of particle backscatter coefficient at three wavelengths observed with lidar on 20–21 June 2014, 2310-0210 UTC (signal averaging period), and (b) cirrus ice crystal depolarization ratio (solid lines, volume depolarization ratio as dashed lines) at three wavelengths. **At 1064 nm the volume depolarization ratio is equal to the particle depolarization ratio.** The vertical signal smoothing length is 200 m. Error bars show the relative uncertainty in the retrievals (one standard deviation).
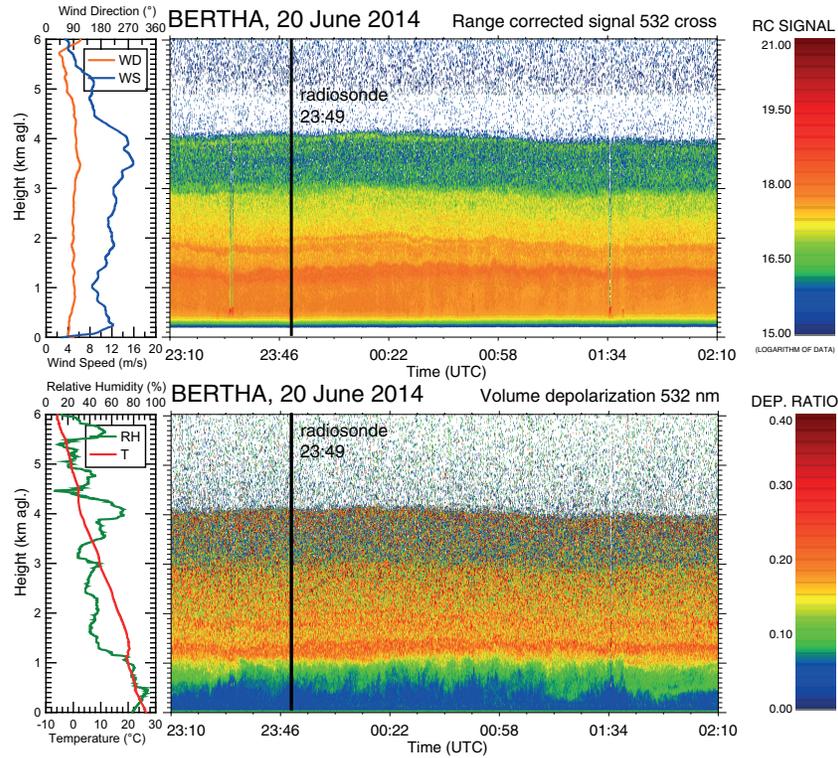
Figure 7. Saharan air layer (from 1–4 km height) above the marine boundary layer. The same parameters as in Fig. 2 are shown.The lidar observation was performed on 20 June 2014, 19:10–22:10 local time. The radiosonde was launched at 19:46 local time (indicated by black vertical lines).
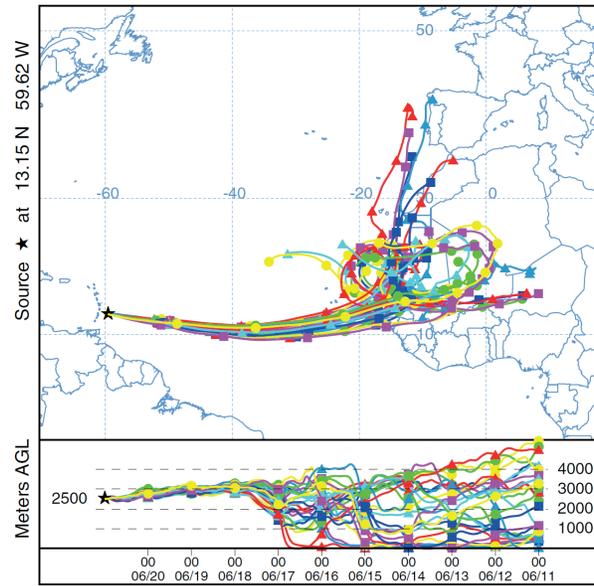
Figure 8. Ensemble of 10-day HYSPLIT backward trajectories for 21 June 2014, 00:00 UTC, arriving at at 2500 m over Barbados.
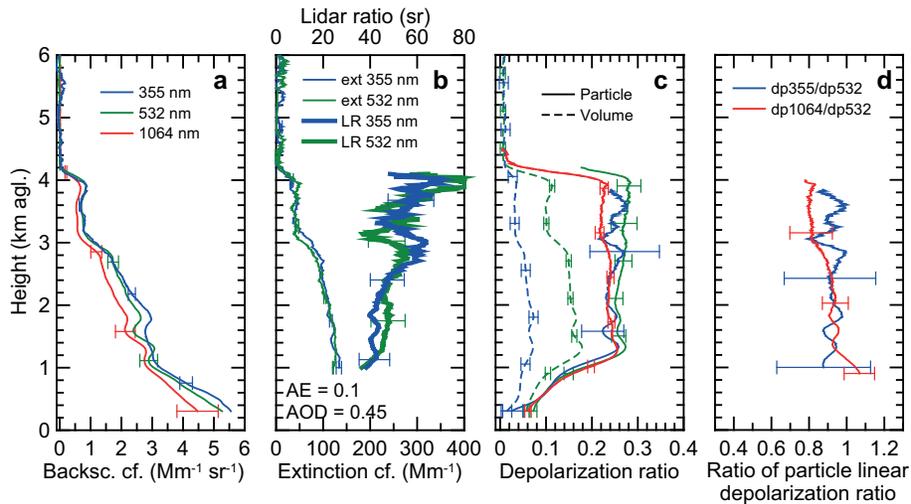
Figure 9. 3-hour mean profiles of (a) the particle backscatter coefficient at three wavelengths, (b) extinction coefficient and lidar ratio at two wavelengths, (c) volume and particle linear depolarization ratio at three wavelengths, and (d) ratio of the 355 nm to 532 nm and 1064 nm to 532 nm particle depolarization ratio. The lidar observation was performed on 20–21 June 2014, 23:10–02:10 UTC. The vertical signal smoothing window length is 200 m (backscatter coefficient, depolarization ratio) and 750 m (extinction coefficient, lidar ratio). Error bars indicate the retrieval uncertainty.
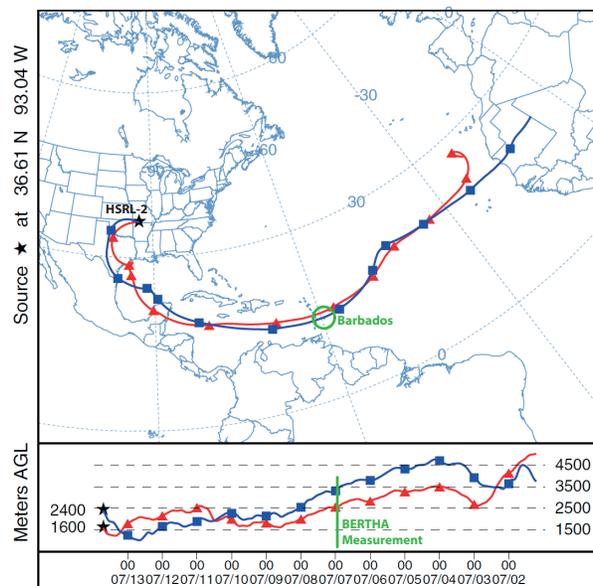
Figure 10. 12.5-day HYSPLIT backward trajectories for 13 July 2014, 17:00 UTC, arriving at at 1600 m (red) and 2400 m (blue) over northern **Missouri** (Midwestern United States). The location (Barbados) and time of the corresponding BERTHA lidar measurement is indicated by a green vertical line.
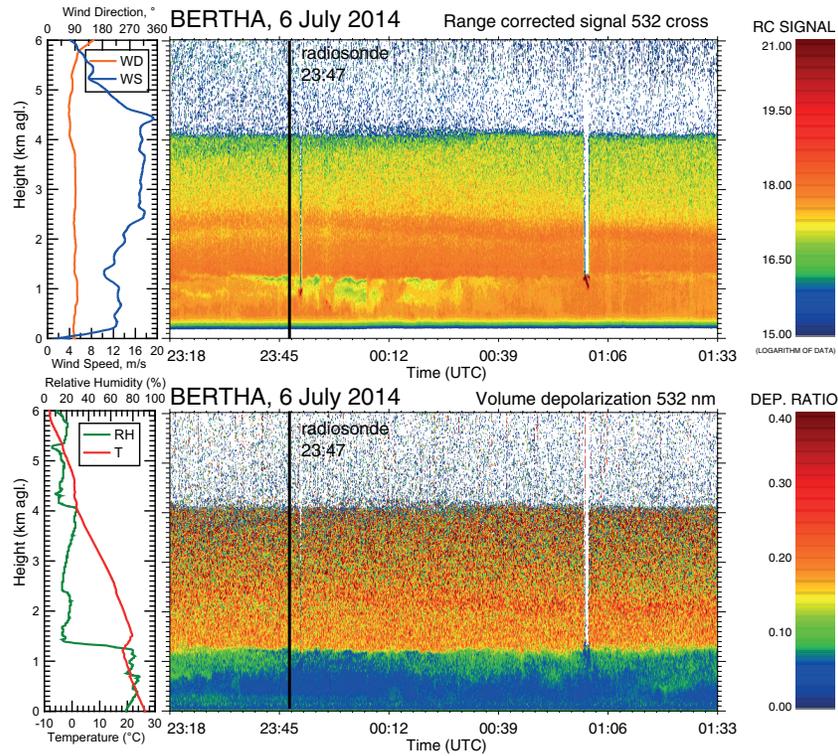
Figure 11. Saharan air layer (from 1.2–4.2 km height) above the marine boundary layer. The same parameters as in Fig. 2 are shown. The lidar observation was performed on 6 July 2014, 19:18–21:33 local time. The radiosonde was launched at 19:47 local time (indicated by a black vertical line).
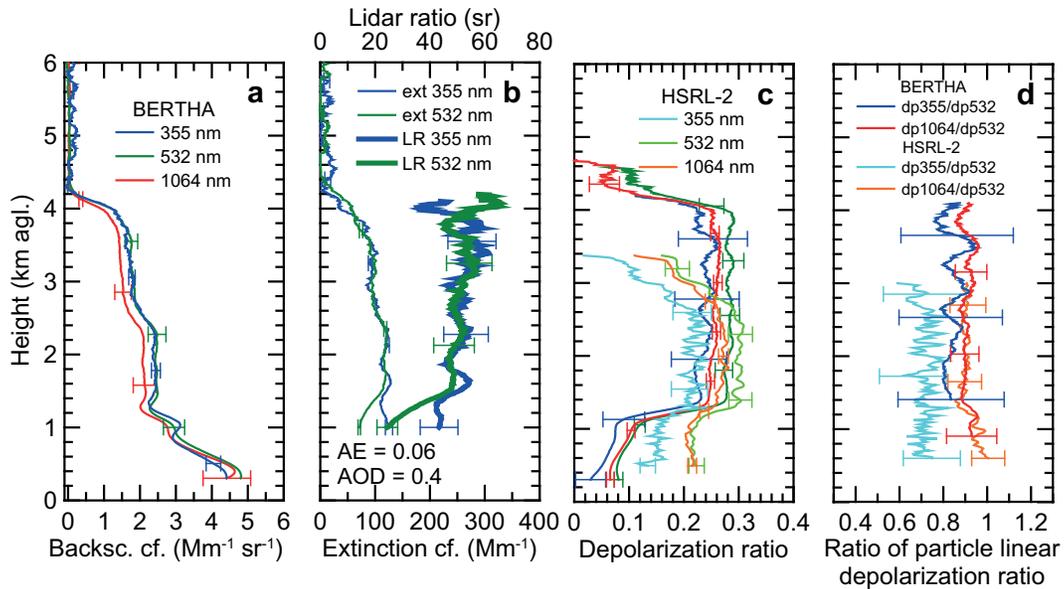
Figure 12. Same as Fig. 9, except for 6–7 July 2014, 23:18–01:33 UTC. For comparison, respective height profiles of the particle linear depolarization ratio (355 nm in light blue, 532 nm in light green, and 1064 nm in orange and for the ratio of depolarization ratios (in light blue and orange) measured with an airborne triple-wavelength polarization lidar (HSRL-2) (Burton et al., 2015) on 13 July 2014, 1700 UTC are shown. The airborne lidar observations were performed in **Missouri** (Midwestern United States), about 7000 km and 7 days downwind of Barbados.
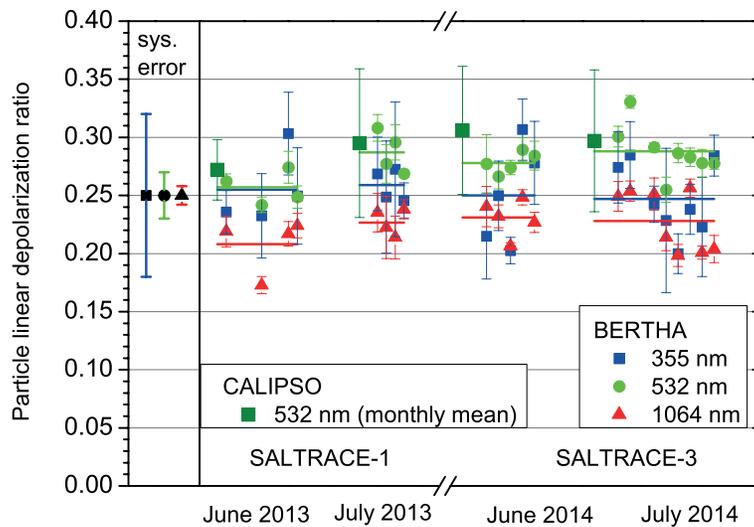
Figure 13. Overview of SAL **layer mean** particle depolarization ratios measured with triple-wavelength polarization lidar BERTHA during SALTRACE-1 (2013) and SALTRACE-3 (2014). Only triple-wavelength observations (one per evening) are considered. Horizontal lines show the mean values of all measurements conducted in one of the four SALTRACE months in 2013 and 2014. Error bars indicated the standard deviation calculated from all depolarization values (available with 50 m vertical resolution) between SAL base and top. Respective CALIOP monthly mean values and standard deviations of the SAL column particle depolarization ratios at 532 nm are shown for comparison. Level 2 version 3.30 CALIPSO Aerosol profile data around Barbados are used for this retrieval (CALIPSO, 2016). The systematic error bars shown on the left-hand side illustrate the impact of all the made retrieval assumptions on the results.

45
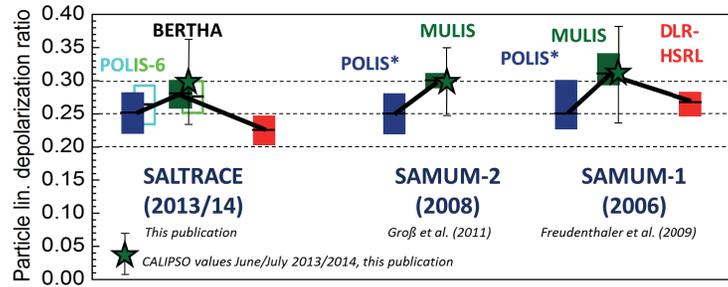
Figure 14. Comparison of dust-layer mean particle linear depolarization ratios measured during SAMUM-1 (Morocco), SAMUM-2 (Cabo Verde), and SALTRACE (Barbados). Colored bars show the range of mostly observed depolarization ratios at 355 nm (blue), 532 nm (green) and 1064 nm (red). The lidars BERTHA, POLIS, MULIS (the second polarization lidar of Munich University), and the airborne High Spectral Resolution Lidar (HSRL) of DLR (Deutsches Zentrum für Luft- und Raumfahrt) were used to collect this data set. Data are taken from the publications of (Freudenthaler et al., 2009) (SAMUM-1, **19 cases for MULIS, less for the other systems (2-4)**), (Groß et al., 2011a) (SAMUM-2, **9 cases for POLIS, 5 cases for MULIS**), (Groß et al., 2015) (SALTRACE, POLIS-6) and from this study (21 cases). In addition, CALIOP mean values of SAL column depolarization ratios considering all observations during the four SALTRACE months (June and July in 2013 and 2014) are shown. The mean values consider all CALIOP overpasses of selected areas in southeastern Morocco, in the Cabo Verde region, and around Barbados during these four months.
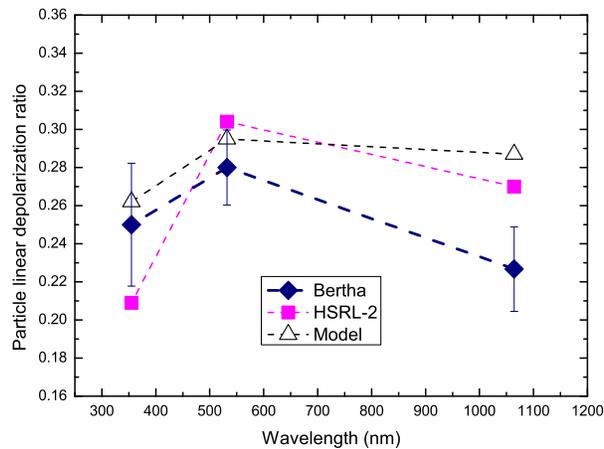

Figure 15. SALTRACE mean dust particle linear depolarization ratios at 355, 532, and 1064 nm (SAL column mean values and corresponding standard deviations) measured with BERTHA (21 cases). In addition, the HSRL-2 observation (Burton et al., 2015)) discussed in Sect. 3.3 is shown. The observational findings are compared with respective model results which are based on the dust size-shape characteristics described in Gasteiger et al. (2017).

46
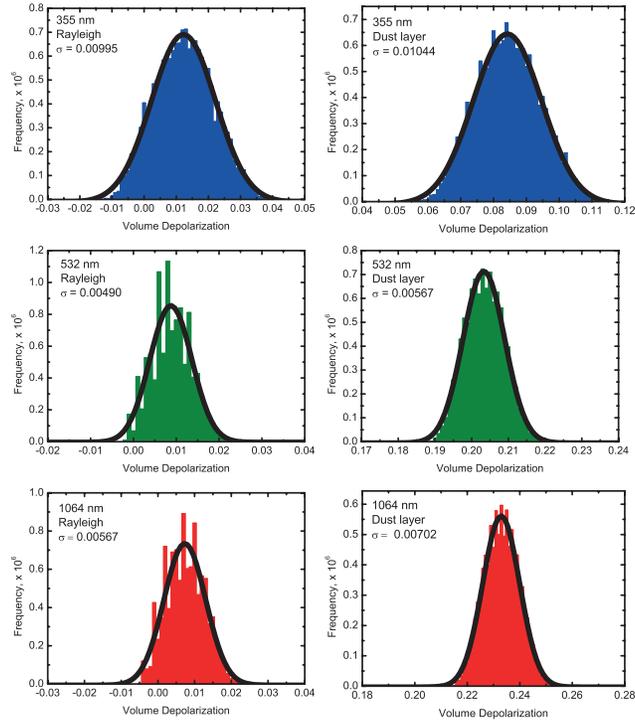
Figure 16. Frequency distribution (in millions of individual computations) of the volume depolarization ratio derived by a Monte-Carlo simulation of the system parameters of the BERTHA lidar system (Tab. 3) within their uncertainties. For each wavelength the Rayleigh depolarization and a typical value in the dust layer was chosen as the input value (true value), given in Table 4. The standard deviation σ of the Gaussian fit (black line) is given to estimate the error of the volume depolarization ratio.